Journal of Hydrology 583 (2020) 124629

Contents lists available at ScienceDirect

Journal of Hydrology

journal homepage: www.elsevier.com/locate/jhydrol

Research papers

Interpolated or satellite-based precipitation? Implications for hydrological modeling in a meso-scale mountainous watershed on the Qinghai-Tibet Plateau

Ling Zhang[a,*], Dong Ren[b], Zhuotong Nan[c], Weizhen Wang[a], Yi Zhao[c], Yanbo Zhao[a], Qimin Ma[a], Xiaobo Wu[d]

[a] Key Laboratory of Remote Sensing of Gansu Province, Northwest Institute of Eco-Environment and Resources, Chinese Academy of Sciences, Lanzhou 730000, China
[b] Hydrology Water Resources Bureau of Gansu Province, Lanzhou 730000, China
[c] Ministry of Education Key Laboratory of Virtual Geographic Environment, Nanjing Normal University, Nanjing 210023, China
[d] College of Resources and Environment, Sichuan Agricultural University, Chengdu 611130, China

ARTICLE INFO

This manuscript was handled by Marco Borga, Editor-in-Chief, with the assistance of Francesco Marra, Associate Editor

Keywords:
Interpolation
Hydrological modeling
Mountainous watersheds
TMPA
IMERG
DHSVM

ABSTRACT

The interpolation algorithms and the satellite-based precipitation products (SPPs) are two major approaches to estimating spatially distributed precipitation. This would inevitably raise the questions: whether the interpolation algorithms could outperform the SPPs or vice versa? And what's the implications for hydrological modeling? These questions, however, have received little attention in the literature. This study compared the performances of two quasi-physically based interpolation algorithms (i.e., MicroMet and PrecLaps) with the widely used SPPs, i.e., Tropical Rainfall Measuring Mission Multisatellite Precipitation Analysis (TMPA) and Integrated Multi-Satellite Retrievals for Global Precipitation Measurement (IMERG), in and around the Babao River Basin (BRB), a meso-scale mountainous watershed on the Qinghai-Tibet Plateau. Meanwhile, the hydrological utilities of the interpolated and the satellite-based precipitation were evaluated by using the Distributed Hydrology Soil Vegetation Model (DHSVM). Results indicate that TMPA and IMERG perform worse than the interpolation algorithms in estimating daily precipitation, while they show comparable and even higher performance in reproducing monthly precipitation. Both the interpolation algorithms and the SPPs have an obvious lower performance in winter than the other seasons. DHSVM with the TMPA-based or IMERG-based precipitation, when not subjected to additional calibration, performs worse than those with the interpolated precipitation in simulating streamflow. Nevertheless, interestingly, the ET simulations consistently match well with the independent remote sensing (RS)-based ET product, as indicated by the higher coefficient of determination ($R^2 \geq 0.85$) and Nash-Sutcliffe efficiency ($NSE \geq 0.72$). The additional calibration of DHSVM with the satellite-based precipitation could enhance the streamflow simulation accuracy substantially, with the *NSE* increasing by 70.59–132% in the validation period. This, however, would bring about larger discrepancies between the simulated and the RS-based ET in summer. The study further discussed the implications of these findings for hydrological modeling over the data-scarce mountainous watersheds, and revealed the uncertainties associated with the rain gauge density.

1. Introduction

Precipitation is one of the key factors affecting watershed hydrology and water resource systems. It varies significantly both in space and time (Bárdossy and Pegram, 2013). Hence, accurate and reliable information regarding the temporal and spatial variabilities of precipitation are of vital importance for a wide range of applications (Camera et al., 2014; Sun et al., 2018) such as hydrological and ecological modeling (Lima et al., 2018), water resource managements (Supit et al., 2012), flood and drought monitoring (Hui-Mean et al., 2018; Yuan et al., 2019), and terrestrial ecosystem studies (Gritti et al., 2006; Mo et al., 2019).

Rain gauge is the traditional method used to measure precipitation at the point scale of the Earth's surface (Li et al., 2018). Theoretically, the spatial patterns of precipitation at the basin or regional scales can be well captured if the gauge networks are dense enough.

* Corresponding author.
E-mail address: zhanglingky@lzb.ac.cn (L. Zhang).

https://doi.org/10.1016/j.jhydrol.2020.124629
Received 10 September 2019; Received in revised form 21 January 2020; Accepted 24 January 2020
Available online 28 January 2020

Nomenclature

Acronyms

BRB	Babao River Basin
PrecLaps	Precipitation lapse
SPPs	Satellite-based precipitation products
DHSVM	Distributed Hydrology Soil Vegetation Model
MicroMet	Meteorological Distribution System for High-Resolution Terrestrial Modeling
TMPA	Tropical Rainfall Measuring Mission (TRMM) Multisatellite Precipitation Analysis
IMERG	Integrated Multi-Satellite Retrievals for Global Precipitation Measurement

Unfortunately, in reality, the rain gauges are usually sparsely and unevenly distributed, particularly in some less developed regions as well as the remote mountainous areas (Duan et al., 2019). Consequently, the interpolation algorithms are typically used together with the ground-based measurements to derive spatially distributed precipitation (Tobin et al., 2011; Camera et al., 2014; Huang et al., 2019). To date, various interpolation schemes have been proposed and developed, ranging from the simplest deterministic approach such as the Thiessen polygon and inverse distance weighting (IDW) methods, to the intermediate-complexity approaches such as the MicroMet (Liston and Elder, 2006) and precipitation lapse (PrecLaps) algorithms which take into account the effects of topography, and to some other more complexed geostatistical methods such as the Kriging. The performance of the interpolation algorithms depends on many factors (Hwang et al., 2012) such as the spatio-temporal scales of the precipitation estimates, the mechanism of the methods, the gauge density as well as the topographic features. In recent years, many efforts have been devoted to compare the performance and the hydrological influences of different spatial interpolation techniques. Camera et al. (2014) assessed the performance of 15 interpolation techniques in reproducing daily precipitation over topographically complex areas, and reported that their relative ranks are closely associated with the station density and rainfall amounts. Xu et al. (2015) compared three interpolation techniques for daily rainfall estimations in Sichuan Province of China, and concluded that the ordinary CoKriging (CK) is the optimal method. Zhang et al. (2017a) found that the physically based inverse distance and elevation weighted (PBIDEW) method is more suitable than the inverse distance weighted (IDW) method in estimating precipitation for hydrological modelling in the topographically complex mountainous watersheds. Huang et al. (2019) found that the interpolation approach based on the information diffusion principle and the IDW and geostatistical interpolators provide similar spatial distributions for annual precipitation. Ossa-Moreno et al. (2019) compared the interpolation approaches of different complexities in the upper Aconcagua catchment in central Chile, and recommended the utilization of the method based on the residuals between observations and WorldClim data or Climate Hazards Group Infrared Precipitation with Station (CHIRPS) data. Besides the rain gauge, weather radar is another ground-based tool used to measure precipitation across large domains with fine spatiotemporal resolutions. However, it involves a lot of problems such as the ground clutter and beam blockage, the calibration of the relations between reflectivity and rainfall intensity for different types of precipitation, and the limited distributions around the globe (Delrieu et al., 2009; Sun et al., 2018).

In addition to the ground-based observations, the satellite-based precipitation products (SPPs) emerge as an additional and promising approach to reproduce the spatial patterns of precipitation at the basin, regional and global scales. Since the Tropical Rainfall Measuring Mission (TRMM), a joint mission between the National Aeronautics and Space Administration (NASA) of the United States and the Japan Aerospace Exploration Agency (JAXA), was launched in 1997 (Kummerow et al., 1998), a series of SPPs have been developed and are freely available to the public. Among them, Tropical Rainfall Measuring Mission (TRMM) multi-satellite precipitation analysis (TMPA) (Huffman et al., 2007) and its successor Integrated Multi-Satellite Retrievals for Global Precipitation Measurement (IMERG) (Huffman et al., 2014) are perhaps the most widely used ones in a variety of researches and operational applications. Nevertheless, they are inherently subjected to some systematic and random errors, arising from the retrieval algorithms, the shortcomings of the instruments, the indirect measurements and the sampling uncertainties (Bharti and Singh, 2015; Li et al., 2015; Ebrahimi et al., 2017). Hence, a region-specific assessment is an essential step before their applications.

Currently, numerous studies have evaluated the performances of the TMPA and IMERG products over different regions of the world at various spatio-temporal scales by directly comparing them against the ground-based observations (Bharti and Singh, 2015; Yong et al., 2015; Xu et al., 2017; Beck et al., 2019), or by the indirect modeling-based inference with a focus on hydrological utilities or operational flood modeling (e.g. Li et al., 2015; Camici et al., 2018; Belabid et al., 2019; Duan et al., 2019; Yuan et al., 2019). In particular, the researchers in the field of hydrometeorology have given much attention to the performance of TMPA and IMERG over the mountainous areas where the spatial patterns of precipitation are typically not well captured by the ground-based observations due to the paucity of rain gauges and the strong complexity of the climatic conditions. Meng et al. (2014) evaluated the hydrological utilizes of the TMPA-3B42V6 product in the source region of Yellow River, and proved that it is not suitable for long-term hydrological predictions. El Kenawy et al. (2015) assessed the TMPA-3B42 product over north-eastern Iberia and highlighted the needs of further improvements of the precipitation retrieval algorithms over the areas of heterogeneous terrain. Bharti and Singh (2015) validated the TMPA 3B42V7 product over the Himalayan region, and concluded that it exhibits a better performance for the lower-altitude regions but exacerbates over the higher-altitude ones. Kim et al. (2016) reported that TMPA is applicable for hydrological modeling in the mountainous region of South Korea. Ebrahimi et al. (2017) evaluated the performance of the TMPA 3B42 product over the Tibetan Plateau, and demonstrated that it has deficiency in capturing daily precipitation. Yuan et al. (2017) reported the feasibility of the bias corrected IMERG and TMPA 3B42V7 products in hydrological simulations in a data-sparse mountainous watershed in Myanmar. Khan et al. (2018) suggested that the utilization of TMPA product for watershed hydrological simulation is a valuable alternative in data-scarce regions, like the Upper Indus Basin. Wang et al. (2019) evaluated and compared the IMERG (V05B) and TMPA 3B42V7 products under over the Hexi Region with complex terrains in northwest China, and concluded that they underestimate precipitation in the high-altitude mountainous areas. These studies could contribute valuable information to both the data users and producers. Nevertheless, there are obviously conflicting results regarding the performance and the hydrological utilities of the TMPA and IMERG products over the mountainous watersheds, which calls for further investigations.

From the literature reviews, it is very clear that, in most cases, the performance of the interpolation algorithm and the SPPs were assessed separately in the past. However, since both of them are the commonly used methods to deriving spatially distributed precipitation, a key driving variable for distributed hydrological models, it would inevitably raise two important questions: (i) whether the interpolation algorithms could outperform the SPPs or vice versa, especially over the data-scarce mountainous areas? and (ii) what's the implications for hydrological modeling? To our best knowledge, however, there questions have been given rare attention in the literature. Hence, the primary objectives and motivations of this study are (i) to compare the performances of two quasi-physically based interpolation algorithms (i.e., MicroMet and PrecLaps) with the widely used SPPs (i.e., TMPA 3B42V7 and IMERG)

in and around the Babao River Basin (BRB), a meso-scale mountainous watershed on the northeast Qinghai-Tibet Plateau; and meanwhile, (ii) to assess the hydrological utilities of the interpolated and the satellite-based precipitation through the modeling experiments by using the Distributed Hydrology Soil Vegetation Model (DHSVM). The rest of the paper is organized as follows. After the introduction, the study area and data are briefly described in Section 2. Section 3 presents the methodology used in this research. The results and discussion are arranged in Section 4 and Section 5, respectively; and the conclusions are summarized in the last section.

2. Study area and data

2.1. Study area

The Heihe River Basin (HRB) is a typical endorheic river basin in the arid region of northwest China. Its upstream area, lying between 98.0°E–101.3°E and 38.0°N–42.0°N, is located on the northeastern Qinghai-Tibetan Plateau. The Babao River Basin (BRB), which is the eastern tributary of the upstream HRB, was focused in this study (Fig. 1). It serves as a good case study considering that it is a typical mountainous watershed within which only one national-level meteorological station (G03) exists. The BRB is a meso-scale watershed with a drainage area of approximately 2,500 km^2. It is characterized by complex terrains, and has elevations ranging from 2686 m to 4916 m above sea level. The basin has a continental alpine semi-humid climate with an annual precipitation ranging 270–600 mm/year and a mean annual temperature less than 1 °C (Zhang et al., 2017b). Snowfall is an important component of precipitation in the cold season (winter); and the spring snowmelt plays an important role in streamflow generations in the BRB (Wang et al., 2015). As shown in Fig. 1, there are seven vegetation types within the study area, of which the alpine meadow, alpine sparse vegetation (APS) and shrub account for approximately 90% of the total study area. The soil textures include sandy loam, loam, and silt/silt loam (Lu et al., 2011); and the soil depth exhibits a strong spatial variability, varying from 5.66 to 180 cm (Song et al., 2016; Yang et al., 2016).

2.2. Data

As listed in Table 1, three categories of data were used in this study. The first one mainly includes the data used for model setup and

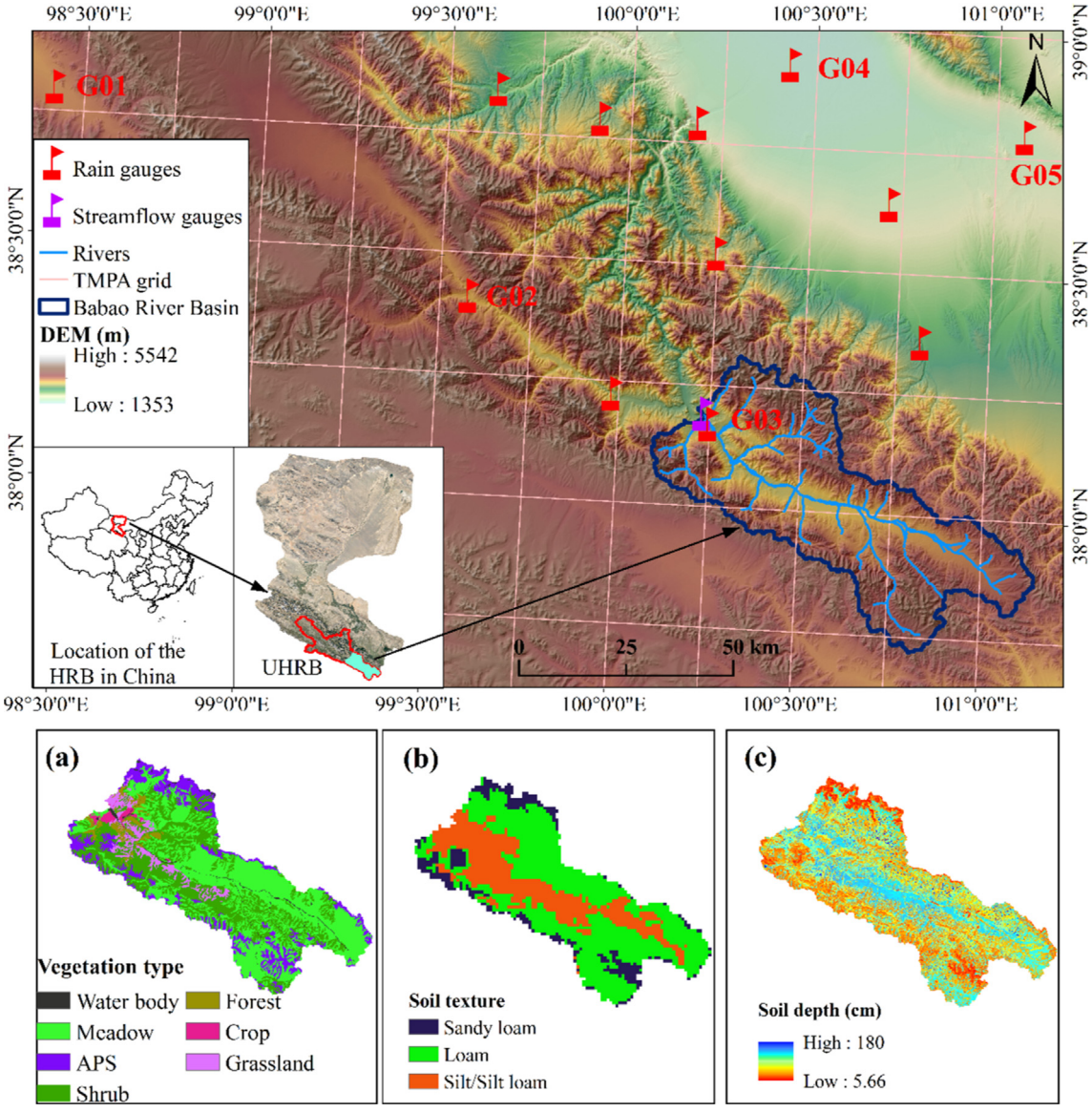

Fig. 1. Location of the Babao River Basin (BRB) and the maps of vegetation (a), soil texture (b) and soil depth (c).

Table 1
Data used in this study.

Category	Data	Spatial resolution	Source
Model setup and parametrization	Meteorological data	12 station	NMIC/WRBGP
	DEM	90 × 90 m	ASTER GDEM
	Vegetation map	1:100,000	SDCCAR
	Soil texture	1 km	SDCCAR
	Soil depth	90 m	SDCCAR
	Soil hydrological parameters	90 m	SDCCAR
	LAI	1 km	SDCCAR
Model calibration and validation	Streamflow	1 station	WRBGP
	RS-based ET	1 km	SDCCAR
Modeling experiments	TMPA 3B42 (Version 7)	0.25°	GES DISC
	IMERG (Version 6)	0.10°	GES DISC

parametrization. The meteorological forcing data of five national-level stations (Fig. 1, G1-5), including maximum and minimum temperature, precipitation, relative humidity and wind speed, were obtained from the National Meteorological Information Center (NMIC) (http://data.cma.cn/). In addition, the observations from another seven local rain gauges were further collected from the Water Resources Bulletin of Gansu Province (WRBGP) (http://www.gssl.gov.cn/). The 90-m local Digital Elevation Model (DEM), clipped from the ASTER Global DEM, was used to define the topography and generate stream map and network. The 1:100,000 vegetation map (Zhang et al., 2018c), the patterns of soil texture (Lu et al., 2011) and soil depth, and the data of soil hydrological properties (Song et al., 2016; Yang et al., 2016) were used to define the vegetation and soil types, and to parametrize the soil physical characteristics. Meanwhile, the leaf area index (LAI) data at the spatial resolution of 1 km, which was reconstructed from the MODIS NDVI product through the Harmonic Analysis of Time Series (HANTS) algorithm (Jia et al., 2011), was adopted to estimate the monthly LAI. All the data of the first category except for the meteorological data were collected from the Science Data Center for Cold and Arid Regions (SDCCAR) (http://westdc.westgis.ac.cn). The data of the second category were mainly used for model calibration and validation. The daily streamflow observations at the outlet of the BRB (i.e., the Qilian station) were obtained from the WRBGP for the period 1998–2013. Besides, the Remote Sensing (RS)-based product, which was derived through an operational software system (ETWatch) for regional evapotranspiration (ET) monitoring (Wu et al., 2012), was used to crosscheck the simulations of DHSVM.

The data of the last category, i.e., the TMPA 3B42 and IMERG products, were used for the modeling experiments. The TMPA 3B42 product covers the quasi-global areas ranging 50° N-50° S with a 0.25° × 0.25° spatial resolution and a 3-hourly temporal resolution from January 1998 to present, while its successor IMERG covers the globe with a higher spatial and temporal resolutions (0.1° × 0.1°, 30 min) from June 2000 to present. The key advancement of IMERG over TMPA is the extended capability to capture solid precipitation and light rain (< 0.5 mm h^{-1}). The latest versions of the post-real-time TMPA 3B42 and IMERG products for the period 2001–2014 were used in this study, and would be simply referred to TMPA and IMERG hereafter for conciseness. These data are provided by the National Aeronautics and Space Administration, and can be freely downloaded from the Goddard Earth Sciences Data and Information Services Center (GES DISC) (https://disc.gsfc.nasa.gov/). As we known, the post-real-time TMPA and IMERG products have been climatologically adjusted month by month using the Global Precipitation Climatology Center (GPCC) monthly full/monitoring gauge product. However, there are only 194 international exchange stations across China within the GPCC network (Sheng et al., 2013; Wang et al., 2018). None of rain gauges used in this research belong to the international exchange stations, leading to an independent assessment of TMPA and IMERG.

3. Methodology

3.1. Quasi–physically based precipitation interpolation algorithms

3.1.1. MicroMet

The Meteorological Distribution System for High-Resolution Terrestrial Modeling (MicroMet) is an intermediate-complexity and quasi-physically based model that was designed to produce high-resolution meteorological forcing distributions based on the relationships between climatic variables and the surrounding landscapes (primarily topography) (Liston and Elder, 2006). It has been widely used to perform meteorological interpolations over the mountainous areas with complex terrains (e.g. Mernild et al., 2017; Cao et al., 2018; Zhang et al., 2018b; Zhao et al., 2019). Within the framework of MicroMet, precipitation is distributed over a spatial domain through a two-step process. First, the observations and elevations of the rain gauges are interpolated horizontally to the model grids by using a Barnes objective analysis scheme which adopts a distance-dependent weighting function (Koch et al., 1983). The weight (w) assigned to a precipitation station is calculated use Eq. 1.

$$w = \exp\left(-\frac{r^2}{f(dn)}\right) \tag{1}$$

where r is the distance between the interpolated grid cell and the rain gauge; and $f(dn)$ is a parameter that defines the shapes of the filter response function, and is determined by the data spacing and distribution (Liston and Elder, 2006). Second, the interpolated precipitations of the model grids are adjusted vertically through Eq. 2.

$$P = P_0\left(\frac{1+\beta(Z-Z_0)}{1-\beta(Z-Z_0)}\right) \tag{2}$$

where P and P_0 are the adjusted and interpolated precipitation, respectively; Z and Z_0 are the actual and interpolated elevations, respectively; and β is the topography-based adjustment factor that varies from month to month.

3.1.2. PrecLaps

The precipitation lapse (PrecLaps) scheme is a relatively simple approach that performs interpolation according to the precipitation lapse rate (i.e., the decrement of precipitation with height) and the elevation difference between the model grid and rain gauge. Specifically, it estimates precipitation at the grid where rain gauge is absent by using Eq. (3).

$$P = \sum_{i}^{Nsta} w_i P_i (1 + \gamma(Z - Z_i)) \tag{3}$$

where P and P_i are the interpolated and measured precipitation, respectively; Z and Z_i are the elevations of the model grid and rain gauge, respectively; w_i is the weight assigned to the rain gauge i, which is estimated through the IDW method; $Nsta$ is the number of gauges used

for interpolation; and γ is the precipitation lapse rate. The PrecLaps algorithm was selected in this research mainly due to its simplicity and more importantly, it is a built-in scheme in DHSVM.

3.2. Performance of the interpolation algorithms and the SPPs

The interpolation algorithms and the SPPs (i.e., TMPA and IMERG) were evaluated by using the gauge-based observations in and around the BRB. In terms of SPPs, the precipitation estimates in the grid that contains the rain gauge were directly compared with the corresponding observations. Regarding the interpolation algorithms, the assessment was conducted by using the leave-one-out cross-validation method. More specifically, one of the rain gauges is left out, for which precipitation was interpolated from the remaining ones, and then verified against the observations. The interpolations were carried out at the daily scale by using the MicroMet and PrecLaps algorithms, respectively. The grid size of the interpolation was set to 0.25° (about 28 km), in consistent with the TMPA product. As shown in Table 2, the topography-based adjustment factor (β) of MicroMet was estimated for each month through the least square fit of Eq. 2; and the precipitation lapse rate (γ) of PrecLaps was derived based on the linear relationship between the mean annual precipitation and the elevations of the rain gauges.

The performance of the interpolation algorithms and the SPPs were quantitatively assessed through the typical statistical measures including (i) the correlation coefficient (*CC*); (ii) relative bias (*Rbias*); (iii) root mean square error (*RMSE*); and (iv) normalized *RMSE* (*NRMSE*), which are defined as in Eqs. 4, 5, 6 and 7, respectively. A higher value of *CC* together with lower absolute values of *Rbias*, *RMSE* and *NRMSE* signify better performance of the interpolation algorithm or the SPPs, and vice versa.

$$CC = \frac{\sum_{i=1}^{n}(P_i^{obs} - P_{obs}^{mean})(P_i - P_{mean})}{\sqrt{\sum_{i=1}^{n}(P_i^{obs} - P_{obs}^{mean})^2}\sqrt{\sum_{i=1}^{n}(P_i - P_{mean})^2}} \quad (4)$$

$$Rbias = \frac{\sum_{i=1}^{n}(P_i - P_i^{obs})}{\sum_{i=1}^{n}P_i^{obs}} \times 100\% \quad (5)$$

$$\mathrm{RMSE} = \sqrt{\frac{1}{n}\sum_{i=1}^{n}(P_i - P_i^{obs})^2} \quad (6)$$

$$NRMSE = \frac{RMSE}{\frac{1}{n}\sum_{i=1}^{n}P_i^{obs}} \quad (7)$$

where P_i and P_i^{obs} are the precipitation estimates of the SPPs (or the interpolation algorithms) and the observations, respectively, at the time step *i*; P_{mean} and P_{obs}^{mean} are the mean values of the precipitation estimates and observations, respectively; and *n* is the number of time steps.

3.3. Distributed hydrology soil vegetation model

3.3.1. Model description

The Distributed Hydrology Soil Vegetation Model (DHSVM) is a high-resolution and process-based hydrological model that describes the dynamics of snow cover, soil moisture, ET, and runoff at the catchment scale (Wigmosta et al., 1994). The model was originally designed for mountainous regions with complex terrains, and its source codes are freely available to the public. The latest version of DHSVM, i.e., version 3.1.2, was selected in this study. DHSVM represents a watershed by a series of regular grids with the same size based on DEM, each of which is assigned with appropriate vegetation and soil parameters. Within the framework of DHSVM, (i) the ET is modeled using a two-layer canopy model; (ii) the snow accumulation and melt are simulated through a mass and energy balance model; (iii) the unsaturated moisture movements through multiple rooting zone soil layers are described by Darcy's Law; (iv) the lateral saturated subsurface flow is routed through a cell-by-cell approach while the overland flow is routed through either the cell-by-cell approach or the kinematic wave model (Zhang et al., 2018a); and (v) the channel flow is modeled using a robust linear storage routing algorithm. More details about the model could be found in Wigmosta et al. (1994), Storck et al. (1998) and Wigmosta and Perkins (2001). DHSVM experienced a rapid development after its born in 1994, and has been widely used for a variety of applications such as the hydrological process modeling (Du et al., 2007; Cuo et al., 2008; Zhang et al., 2016), the hydrological impact assessment (Alvarenga et al., 2018; Zhang et al., 2018b; Yearsley et al., 2019), and the sediment transport simulation (Lanini et al., 2009).

3.3.2. Model setup and calibration

DHSVM was setup with a 150-m spatial resolution to ensure an acceptable computational efficiency. The variable infiltration capacity (VIC) model (Liang et al., 1994) was utilized as a meteorological forcing disaggregator to estimate sub-daily (3-hour) meteorological values from the daily ones in order to meet the general requirement of DHSVM (Zhang et al., 2018b). The built-in PrecLaps algorithm was used to interpolate precipitation across the BRB. The stream map and network were generated using the AML script that is available at the official site of the model (http://dhsvm.pnnl.gov/). The DHSVM model was run for the period 2000–2013 at the sub-daily time scale (i.e., 3 h). The first year (2000) was reserved for model warm-up in order to mitigate the effects of inaccurate initial conditions. The period from 2001 to 2004 was selected as the calibration period, and the remaining one (i.e., 2005–2013) as the validation period.

The calibration of DHSVM was performed through a "trial and error" process. The sensitive parameters of DHSVM were first identified through the global sensitivity analysis algorithm, i.e., the extended Fourier amplitude sensitivity test (EFAST) (Saltelli et al., 1999). We selected eight soil-related parameters (i.e., Lateral Conductivity (LC), Exponential Decrease (ED), Maximum Infiltration (MI), Manning Coefficient (MC), Filed Capacity (FC), and Pore Size Distribution (PSD), Bubbling Pressure (BP), Depth Threshold (DT)), and three vegetation-related parameters (i.e., Leaf Area Index (LAI), Leaf Albedo (LA) and Minimum Resistance (MR)) to conduct the sensitive analysis. As shown in Fig. 2, the identified sensitive parameters include FD, LC, ED, LAI, BP and PSD, for which the global sensitivity indexes are greater than 0.10. These sensitive parameters were divided into two groups: uncalibrated and calibrated ones. The uncalibrated group consists of LAI and FD, which were parametrized according to the available RS-based LAI product (Jia et al., 2011) and the data of soil properties (Song et al., 2016; Yang et al., 2016). They were assumed to be "true", and were not subjected to further calibration. The remaining ones belong to the calibrated group; and each of them was adjusted at a time until the simulations of streamflow at the outlet of the BRB are completely satisfactory.

Table 2
Parameters determined for the interpolation algorithms.

Interpolation algorithms	Parameter
PrecLaps	Precipitation lapse rate (γ, mm/km):144
MicroMet	Monthly adjustment factor (β, km^{-1}): 0.00, 0.09, 0.15, 0.17, 0.20, 0.22, 0.19, 0.21, 0.16, 0.17, 0.00, 0.00

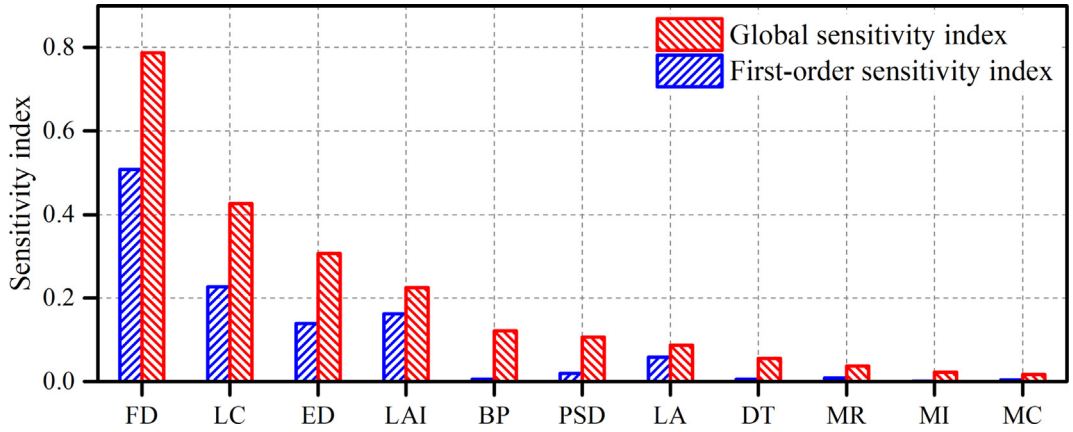

Fig. 2. Global and first-order sensitivity indexes of the soil-related and vegetation-related parameters in DHSVM.

3.4. Hydrological modeling experiments

As shown in Table 3, we designed six modeling experiments to evaluate the hydrological utilities of the interpolated and the satellite-based precipitation. The experiment DHSVM-PrecLaps is in line with the simulations of the calibrated DHSVM, and serves as the baseline scenario. In DHSVM-MicroMet, the precipitation over the BRB were estimated via the MicroMet algorithm, while in the experiments DHSVM-TMPA-UnCal and DHSVM-IMERG-UnCal, they were estimated via the TMPA and IMERG products, respectively. The parameters as well as the other model settings were kept constant for the four experiments (i.e., DHSVM-PrecLaps, DHSVM-MicroMet, DHSVM-TMPA-UnCal and DHSVM-IMERG-UnCal). Besides, we further designed two another experiments (i.e., DHSVM-TMPA-Cal and DHSVM-IMERG-Cal), in which DHSVM with the satellite-based precipitation were subjected to additional calibration. The grid size of DHSVM (150 m) is smaller than that of the precipitation data (0.25° for TMPA and 0.1° for IMERG). In this study, we did not further interpolate the coarse precipitation to the model grid (150 m), and assumed that precipitation is uniform within the coarse grids. The streamflow simulation accuracy of DHSVM was evaluated via the visual hydrograph inspection and the statistical indexes including the *RMSE*, coefficient of determination (R^2) and Nash-Sutcliffe efficiency (*NSE*) (Nash and Sutcliffe, 1970). The *RMSE* is defined in Eq.5; the R^2 is equal to the square of *CC*; and the *NSE* is defined as Eq.8. In addition, the ET simulations were crosschecked with the independent RS-based ET product (Wu et al., 2012).

$$NSE = 1 - \frac{\sum_{i=1}^{n}(Q_i^{obs} - Q_i^{sim})^2}{\sum_{i=1}^{n}(Q_i^{obs} - Q_{mean}^{obs})^2} \quad (8)$$

where Q_i^{obs} and Q_i^{sim} are the observations and simulations, respectively, at time step *i*; Q_{mean}^{obs} is the mean value of the observations; and *n* is the number of time steps.

4. Results

4.1. Evaluations of the interpolation algorithms and the SPPs

Fig. 3 presents the boxplots of the performance metrics (*CC*, *RMSE*, *NRMSE* and *Rbias*) for the SPPs (TMPA and IMERG) and the interpolation algorithms (PrecLaps and MicroMet) at multiple time scales. We can see that the medium *CC* are 0.51 and 0.62, respectively, at the daily scale for the PrecLaps and MicroMet schemes, higher than those for TMPA (0.43) and IMERG (0.50). Meanwhile, the medium *RMSE* and *NRMSE* for the two SPPs are greater than those for the interpolation algorithms. The absolute medium *Rbias* are 10.68% and 5.35%, respectively, for TMPA and IMERG, higher than those for the PrecLaps and MicroMet algorithms, which are 1.20% and 1.98%, respectively. These results indicate the interpolation algorithms perform better than the SPPs in reproducing daily precipitation. At the monthly scale, however, the PrecLaps algorithm performs slightly worse than the TMPA and IMERG product, as indicated by the higher *RMSE* and *NRMSE*. The MicroMet algorithm, which achieves a relatively high medium *CC* (0.93), outperforms TMPA and the PrecLaps algorithm, while it shows a comparable performance with IMERG. At the annual scale, the interpolation algorithms perform better than the SPPs in terms of *CC*, whereas they exhibit lower performance in terms of *NRMSE*. Comparing the results at different time scales, we can see that the interpolation algorithms and the SPPs perform apparently better in estimating monthly precipitation than in reproducing daily and annual ones. It should be mentioned that the PrecLaps algorithm tends to have a higher variability of the performance, in comparison to the MicroMet algorithm and the SPPs, as indicated by the larger ranges of the performance metrics.

Fig. 4 shows the boxplots of the performance metrics in different seasons including spring (March to May), summer (Jun to August), autumn (September to November) and winter (December to February). Similar patterns of the seasonal variations of the performance can be observed for the interpolation algorithms and the SPPs. In terms of *CC*, it shows an increasing trend from spring to summer and autumn, and then drop rapidly in winter. The medium *RMSE* is highest in summer,

Table 3
Modeling experiments designed to evaluate the hydrological utilities of the interpolated and the satellite-based precipitation.

Modeling experiments	Precipitation estimates (spatio-temporal resolutions)	Model parameters
DHSVM-PrecLaps	PrecLaps (0.25°/daily)	—
DHSVM-MicroMet	MicroMet (0.25°/daily)	Same with DHSVM-PrecLaps
DHSVM-TMPA-UnCal	TMPA (0.25°/daily)	Same with DHSVM-PrecLaps
DHSVM-IMERG-UnCal	IMERG (0.10°/daily)	Same with DHSVM-PrecLaps
DHSVM-TMPA-Cal	TMPA (0.25°/daily)	Additional calibration
DHSVM-IMERG-Cal	IMERG (0.10°/daily)	Additional calibration

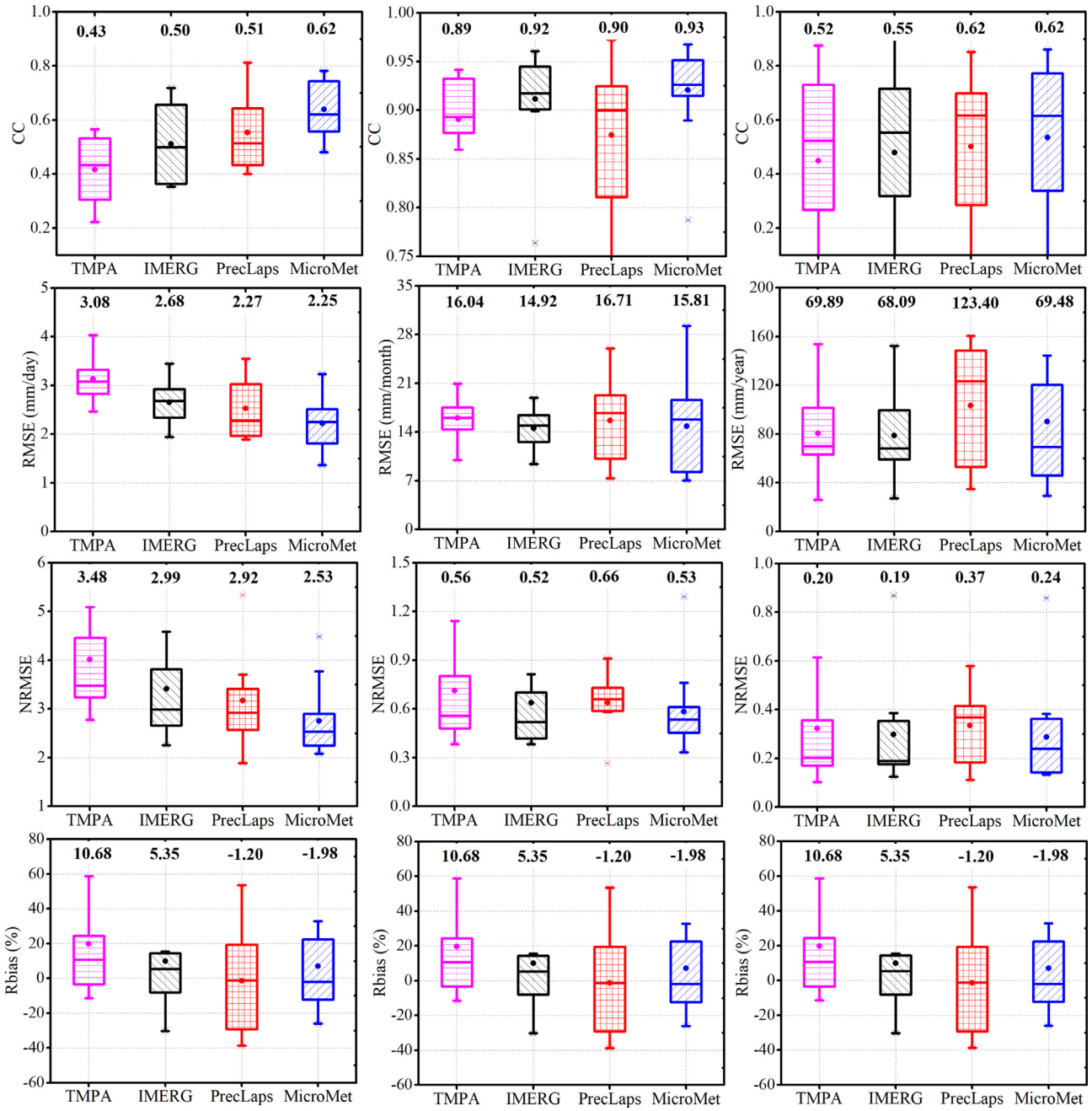

Fig. 3. Boxplots of the performance metrics (*CC*, *RMSE*, *NRMSE* and *Rbias*) for the SPPs (TMPA and IMERG) and the interpolation algorithms (PrecLaps and MicroMet). The median values of the performance metrics are shown at the top of each box. The first, second and last columns present the results at the daily, monthly and annual scales, respectively.

followed by autumn, spring and winter, due to the higher precipitation amounts than the other seasons. The medium *NRMSE*, on the contrary, shows the highest value in winter, followed by spring, autumn and summer. The MicroMet algorithm consistently performs better than IMERG, PrecLaps and TMPA in all the seasons, in terms of *CC*, *RMSE* and *NRMSE*. In winter, the medium *Rbias* is positive and large for TMPA and the interpolation algorithms, indicating an overestimation of precipitation. However, it has a noticeable negative value for IMERG, implying an underestimation of precipitation. Overall, the SPPs and the interpolation algorithms have an obvious lower performance in the cold winter than the other seasons, in line with the findings of the previous studies conducted around our study region (Peng et al., 2014; Yang et al., 2017). The seasonal alterations of the performance metrics at the monthly scale, not presented here, are very similar to those at the daily scale.

4.2. Hydrological simulations in different experiments

Figs. 5 and 6 compare the daily and monthly streamflow observations against the simulations obtained from the modeling experiments at the outlet of the BRB for the period 2001–2013. In the experiment DHSVM-PrecLaps, the simulated streamflow hydrograph exhibits a reasonably good agreement with the observed one. As shown in Table 4, the values of *NSE*, R^2 and *RMSE* are 0.55 (0.65), 0.58 (0.68), and 9.99 (9.53) m^3/s, respectively, for the daily (monthly) streamflow during the calibration period; and they are 0.53 (0.63), 0.56 (0.67), and 9.38 (6.82) m^3/s, respectively, during the validation period. The discrepancies between the simulations and the observations mainly lie in

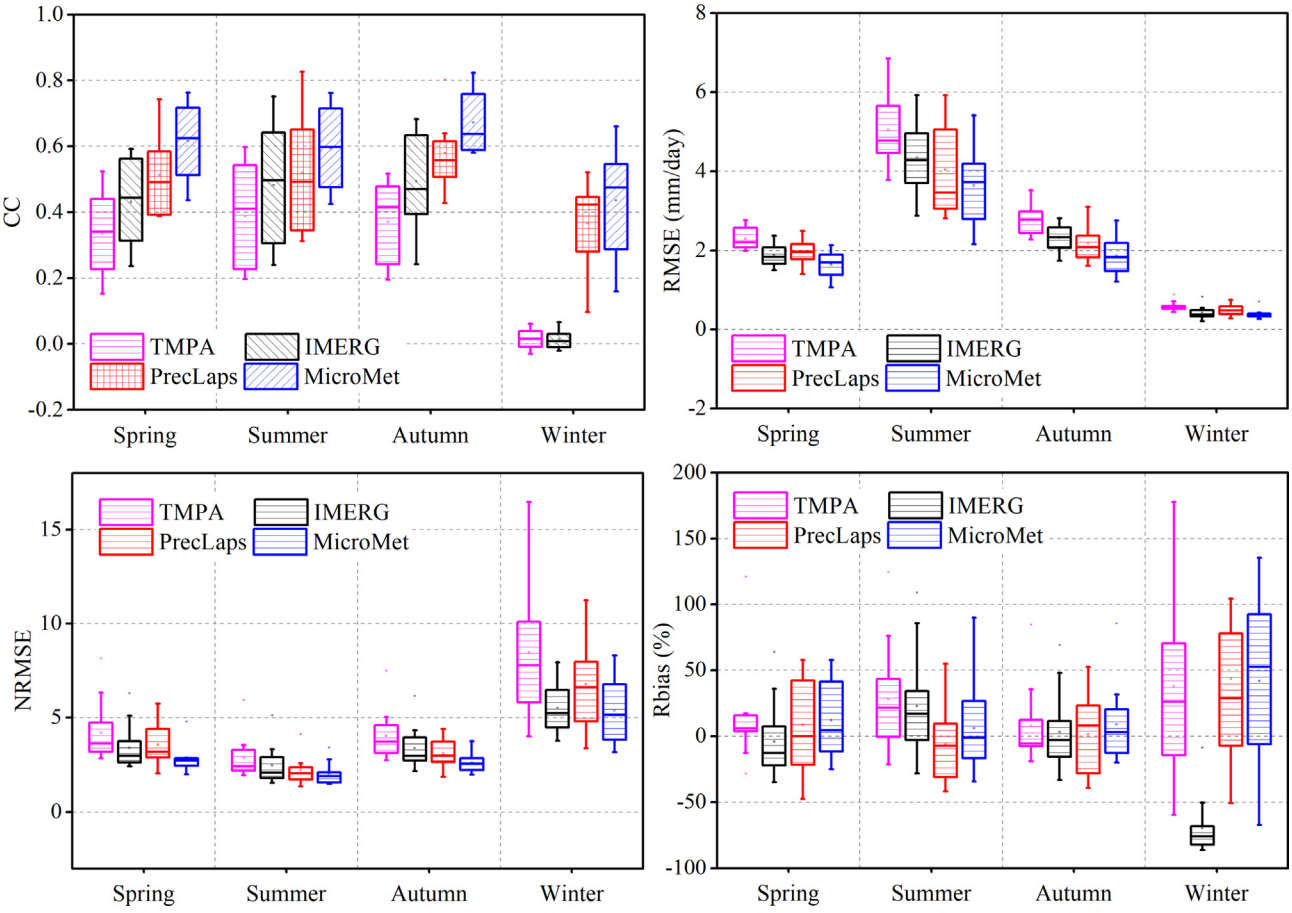

Fig. 4. Seasonal variations of the performance metrics (*CC*, *RMSE*, *NRMSE* and *Rbias*) for the SPPs (TMPA and IMERG) and the interpolation algorithms (PrecLaps and MicroMet) at the daily scale.

the spring streamflow and peak flows. The spring streamflow tends to be underestimated in most of the years. This is possibly due to the absence of the representation of the soil freezing/thawing processes in DHSVM, which plays an important role in the streamflow generations in the BRB. Owing to the freezing process, the water could be preserved in the soil with the form of ice during the cold winter, which would in turn lead to high soil moisture during the warm spring due to the thawing process (Zheng et al., 2018). This could induce high streamflows when confronted with moderate or high precipitation in spring. The peak flows also tend to be underestimated, which might be partially due to the deficiency of DHSVM in representing the preferential flow, and partially due to the exponential decay assumption of the soil lateral saturated hydraulic conductivity (Zhang et al., 2018b). In the experiment DHSVM-MicroMet, the R^2 and *NSE* are slightly higher, and meanwhile, the *RMSE* is lower than those in DHSVM-PrecLaps during the calibration and validation periods. The relatively better performance of DHSVM with the interpolated precipitation of MicroMet is possibly due to the higher precision of the precipitation estimates, as shown in Fig. 3.

In the experiment DHSVM-TMPA-UnCal, the hydrological model could overall reconstruct the variation patterns of streamflow, as indicated by the high R^2 which are 0.53 and 0.71, respectively, for the calibration and validation periods at the monthly scale. Nevertheless, the values of *NSE* are relatively low, which are 0.17 (0.21) and 0.21 (0.25), respectively, during the calibration and validation periods for daily (monthly) streamflow. Meanwhile, the *RMSE* is obviously higher than those in DHSVM-PrecLaps and DHSVM-MicroMet. In the experiment DHSVM-IMERG-UnCal, similarly, the *NSE* and R^2 (or *RMSE*) is significantly lower (or higher) than those in DHSVM-PrecLaps and DHSVM-MicroMet. The streamflow simulation accuracy is even lower than in DHSVM-TMPA-UnCal during the calibration period, but it becomes higher during the validation period. The relatively poor performance of the hydrological model in DHSVM-TMPA-UnCal can be explained by the overestimated summer precipitation of TMPA, particularly in the years 2002–2007, as depicted in Fig. 6a, in comparison to the interpolation algorithms. The poor streamflow simulation precision in DHSVM-IMERG-UnCal, however, is mainly due to the underestimation of precipitation by IMERG over the study region, particularly in the years 2003, 2008 and 2013, which has also been reported by Wang et al. (2019).

The experiments DHSVM-TMPA-Cal and DHSVM-IMERG-Cal are similar to DHSVM-TMPA-UnCal and DHSVM-IMERG-UnCal, respectively, with the exception that DHSVM were subjected to additional calibrations. We can clearly see that, after the further calibration, the streamflow simulation accuracy could be improved significantly. More specifically, the *NSE* could increase from 0.17 (0.21) to 0.32 (0.40) at the daily (monthly) scale in DHSVM-TMPA-Cal during the calibration period, and from 0.21 (0.25) to 0.44 (0.58) during the validation period. In the experiment DHSVM-IMERG-Cal, the *NSE* could increase from 0.04 (0.06) to 0.40 (0.48) at the daily (monthly) scale in the calibration period, and from 0.34 (0.38) to 0.58 (0.71) in the validation period. DHSVM with the TMPA-based precipitation, after the additional calibration, still performs worse than those with the interpolated precipitation. However, DHSVM with the IMERG-based precipitation outperforms those with the interpolated precipitation in terms of streamflow simulation during the validation period, as indicated by the highest *NSE* and R^2, and the lowest *RMSE*.

Fig. 7 shows the comparisons and relations between the

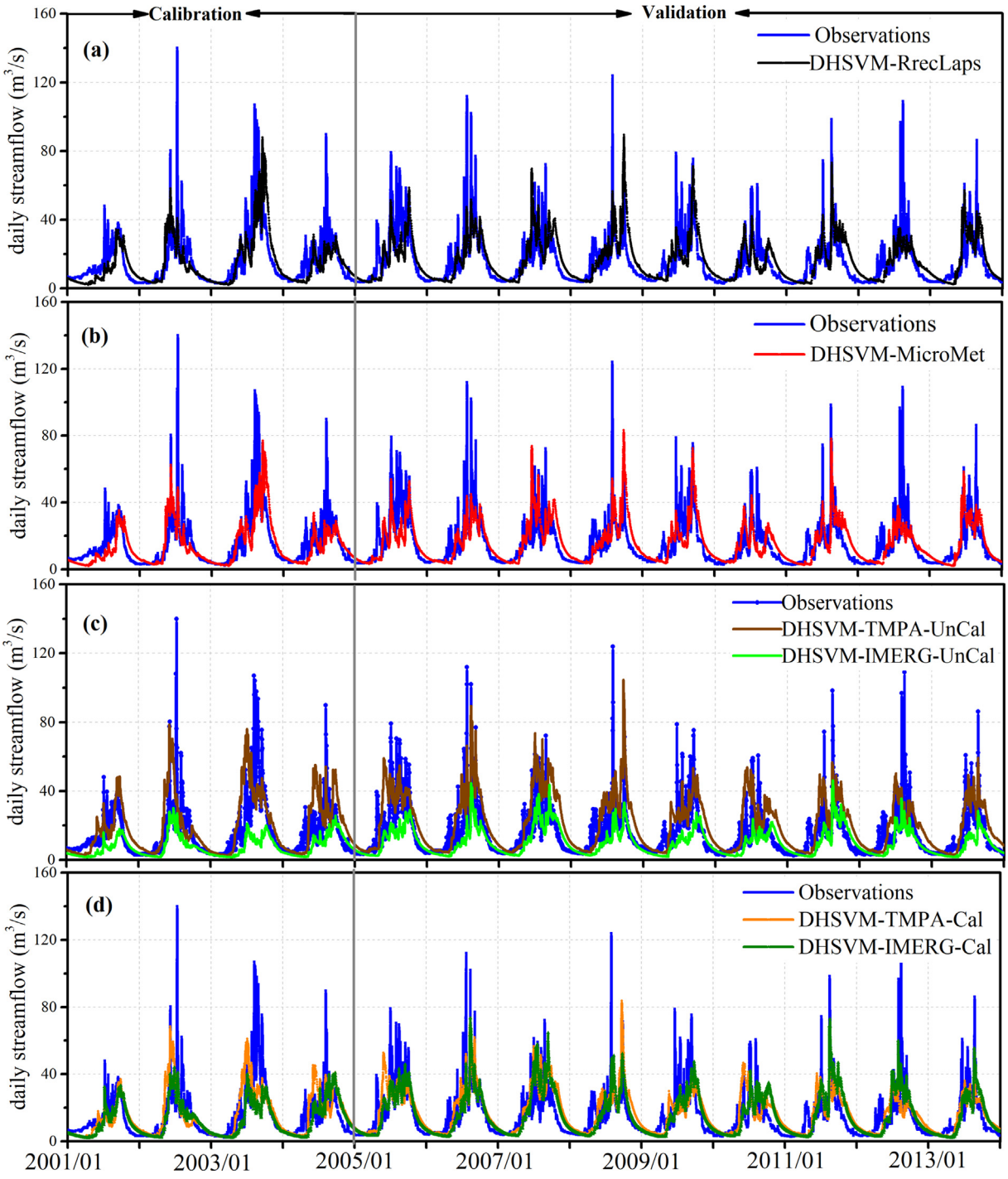

Fig. 5. Comparison of the daily streamflow observations with the simulations generated from different modeling experiments (a, DHSVM-PrecLaps; b, DHSVM-MicroMet; c, DHSVM-TMPA-UnCal and DHSVM-IMERG-UnCal; d, DHSVM-TMPA-Cal and DHSVM-IMERG-Cal) at the outlet of the BRB from January 1, 2001 through December 31, 2013.

independent RS-based ET estimates and the simulations of different modeling experiments for the period 2000–2011. We can see that the variations of the ET could be well captured in the experiments DHSVM-PrecLaps, DHSVM-MicroMet and DHSVM-TMPA-UnCal and DHSVM-IMERG-UnCal, as indicated by the higher R^2 (≥ 0.85) and *NSE* (≥ 0.72). The discrepancies are primarily observed in spring. This is possibly due to the underestimation of soil moisture by DHSVM as mentioned above, which could limit the water available for ET. As plotted in Fig. 7a, b and c, the performance metrics are very close in the experiments DHSVM-PrecLaps, DHSVM-MicroMet, and DHSVM-TMPA-UnCal, implying comparable ET simulations. This is because, on the one hand, the discrepancies between the precipitation estimates of the interpolation algorithms and the TMPA product mainly occur in summer (Fig. 6a), during which, however, the ET are unlikely subjected to water stress. On the other hand, the other climatic factors such as the air temperature and humidity and solar radiation, which could also affect the ET simulations profoundly, were kept consistent for all the experiments. In DHSVM-TMPA-UnCal, the streamflow was overestimated due to the higher precipitation estimates by TMPA. To better match with the streamflow observations, the additional model calibration in DHSVM-

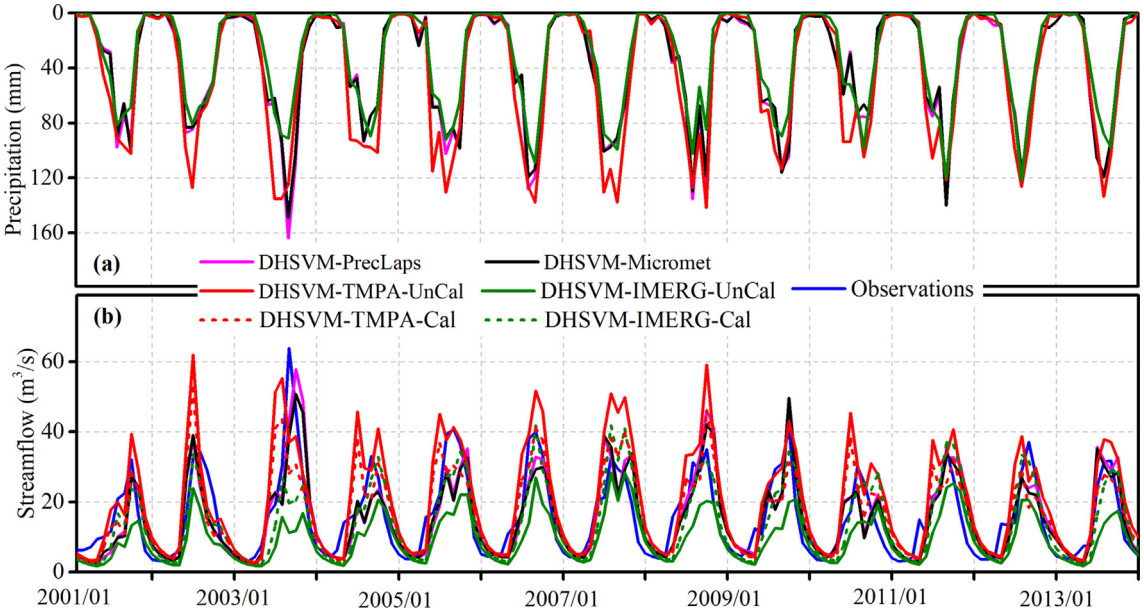

Fig. 6. Comparison of the monthly precipitation estimates (a) and the streamflow simulations (b) in the different modeling experiments.

Table 4
Performance of DHSVM in different modeling experiments during the calibration and validation periods (values outside and in parentheses are the results for the daily and monthly streamflows, respectively).

Modeling Experiments	Calibration period (2001–2004)		
	NSE	R^2	*RMSE* (m^3/s)
DHSVM-PrecLaps	0.55 (0.65)	0.58 (0.68)	9.99 (9.53)
DHSVM-MicroMet	0.57 (0.66)	0.58 (0.68)	9.85 (7.40)
DHSVM-TMPA-UnCal	0.17 (0.21)	0.42 (0.53)	13.61 (11.26)
DHSVM-IMERG-UnCal	0.06 (0.04)	0.37 (0.45)	14.48 (12.39)
DHSVM-TMPA-Cal	0.32 (0.40)	0.38 (0.48)	12.38 (9.82)
DHSVM-IMERG-Cal	0.40 (0.48)	0.45 (0.55)	11.63 (9.16)
Modeling Experiments	Validation period (2005–2013)		
	NSE	R^2	*RMSE* (m^3/s)
DHSVM-PrecLaps	0.53 (0.63)	0.56 (0.67)	9.38 (6.82)
DHSVM-MicroMet	0.54 (0.65)	0.56 (0.67)	9.25 (6.58)
DHSVM-TMPA-UnCal	0.21 (0.25)	0.54 (0.71)	12.16 (9.68)
DHSVM-IMERG-UnCal	0.34 (0.38)	0.50 (0.61)	11.14 (8.79)
DHSVM-TMPA-Cal	0.44 (0.58)	0.48 (0.63)	10.28 (7.52)
DHSVM-IMERG-Cal	0.58 (0.71)	0.59 (0.73)	8.90 (6.05)

TMPA-Cal reduced the simulated streamflow by increasing the ET in summer. Consequently, as marked by the red circle in Fig. 7e, the modeled summer ET tend to be overestimated, and diverge more significantly from the RS-based one in comparison to the experiment DHSVM-TMPA-UnCal, leading to a relatively low *NSE* (0.65). In DHSVM-IMERG-UnCal, the ET simulations agree better with the RS-based ET product than all the other experiments, as indicated by the highest *NSE* (0.81). Nevertheless, the summer streamflow was apparently underestimated in this experiment due to the lower precipitation estimates by IMERG. The further model calibration in DHSVM-IMERG-Cal increased the summer streamflow by decreasing the ET. Hence, as marked by the blue circle in Fig. 7f, the summer ET simulations become more negatively biased in comparison to DHSVM-IMERG-UnCal, resulting in a relatively low *NSE* (0.64).

5. Discussion

5.1. Interpolated or satellite-based precipitation?

The interpolation algorithm and the SPPs are the two major approaches to estimating spatially distributed precipitation, a fundamental input for distributed hydrological models. This study compared and evaluated the interpolation algorithms and the SPPs in estimating precipitation at multiple time scales. We found that the quasi-physically based interpolation algorithms (i.e., PrecLaps and MicroMet) outperform the TMPA product in capturing daily precipitation, particularly in the cold season (winter). The deficiency of TMPA in reproducing daily precipitation has also been reported in some other studies conducted in Qinghai-Tibet Platea (e.g. Ebrahimi et al., 2017; Hussain et al., 2017; Yan et al., 2017), as well as those carried out over the mountainous areas in some other regions such as the upper Indus Basin (Khan et al., 2018), and the Chindwin River basin in Myanmar (Yuan et al., 2017). This might be explained by the following reasons. To begin with, the snow cover within and around the BRB could induce strong scattering in winter, which would lead to overestimations of precipitation by the passive microwave sensor (i.e., TRMM Microwave Imager, TMI) (Ebrahimi et al., 2017; Xu et al., 2017), as indicated by the high positive value of median *Rbias* (26.19%) in Fig. 4. Moreover, the localized and short-term orographic precipitation might not be captured by both the infrared (IR) and passive microwave instruments on-board TRMM (Bharti and Singh, 2015; Xu et al., 2017). Additionally, the other factors such as the time lag and spatial mismatches between the rain gauge and TMPA could also contribute to explain the low performance of TMPA at the daily scale. Hence, the TMPA product cannot be substituted for ground measurements in terms of daily precipitation estimations, as suggested by Camici et al. (2018). Nevertheless, the TMPA product shows a good performance in reproducing monthly precipitation, which is slightly better than the PrecLaps interpolation algorithm. This is partially due to that, as mention in the section of 2.2, TMPA has been subjected to a month-by-month adjustment by using the ground-based observations (i.e., the GPCC data), and partially due to the relatively lower complexities of the monthly precipitation patterns than the daily one. Hence, the TMPA product still has a good potential in the field of hydrometeorology, particularly in the remote mountainous regions without ground-based observations. The low performance of TMPA in capturing daily precipitation but higher performance in estimating monthly precipitation over the mountainous areas have also been reported in many other previous studies (e.g. Ebrahimi et al., 2017; Hussain et al., 2017; Yan et al., 2017; Yuan et al., 2019).

Comparing the two SPPs, IMERG consistently outperforms its predecessor TMPA at the daily, monthly and annual scales, in line with

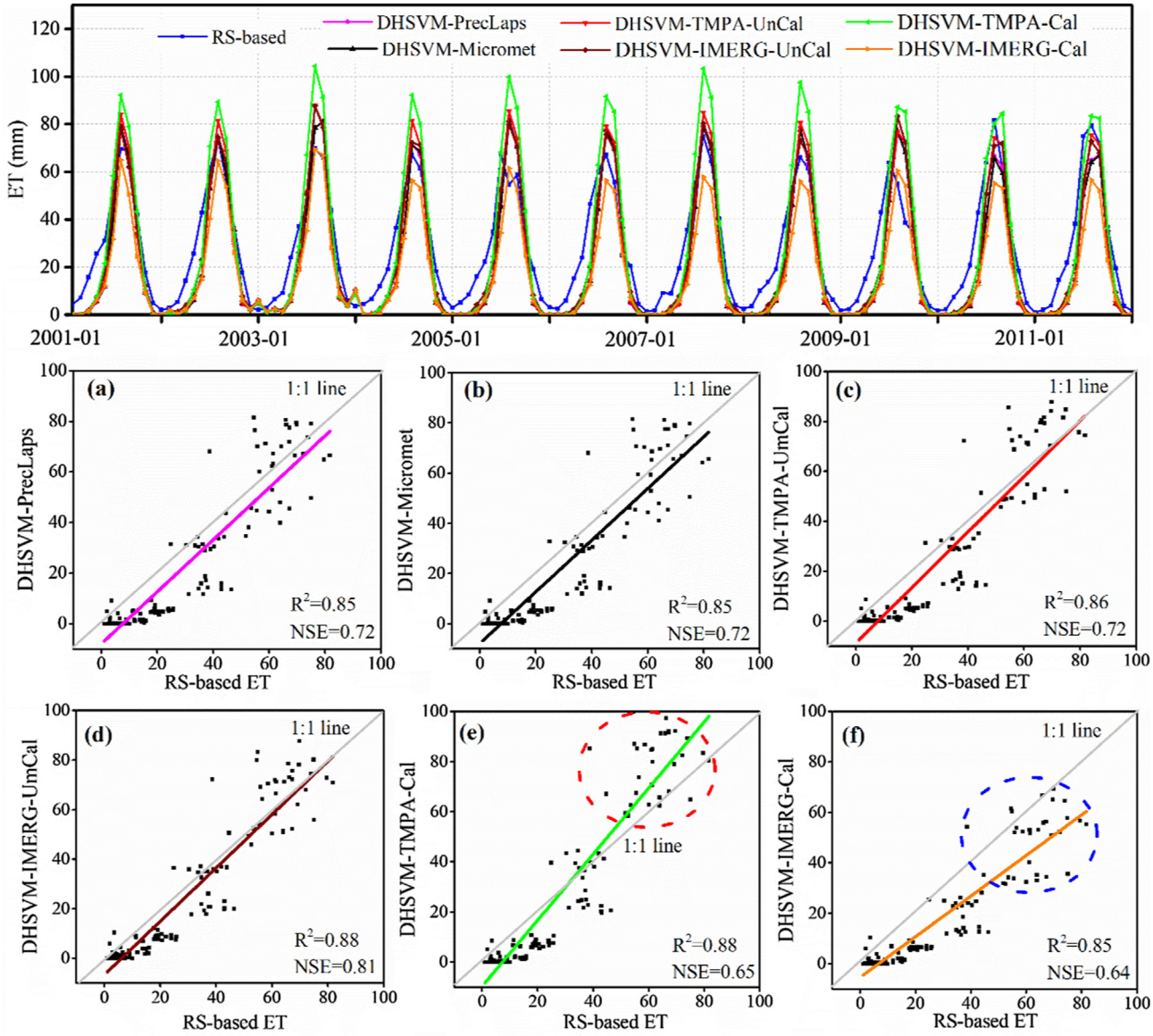

Fig. 7. Comparison of the independent RS-based ET estimations with the simulations generated from different modeling experiments.

many previous studies (e.g. Tang et al., 2016; Xu et al., 2017; Yuan et al., 2018). As a result, the advantage of the interpolation algorithms over IMERG for daily precipitation estimations is smaller than that over TMPA. At the monthly scale, the IMERG product even shows a better and comparable performance in comparison to the PrecLaps and MicroMet algorithms. These results are encouraging, and confirm that IMERG should be a better alternative than TMPA in estimating precipitation over the data-scarce regions. Nevertheless, IMERG doesn't exhibit a better performance than TMPA in winter, as indicated by the relatively low *CC* and higher absolute *Rbias*. This indicates that more efforts are still needed to improve the IMERG product in the cold season over the mountainous areas.

Although the interpolation algorithms outperform the SPPs in estimating daily precipitation, their performance are not very satisfactory as well, mainly due to the deficiencies of the interpolation algorithms. To begin with, the precipitation-elevation relationship, which is derived from the monthly and annual observations, may not be necessarily accurate at the daily scale (Garen et al., 1994). Second, the precipitation frequency tends to be overestimated, owing to that any of the station used for interpolation that have precipitation could lead to the occurrence of precipitation in the interpolated grid cell. This drawback might be mitigated by introducing a precipitation occurrence probability within the framework of the interpolation algorithms, as did by Thornton et al. (1997). In addition, the other factors such as the topographic aspect and slope can also affect precipitation estimates considerably, which, however, are not considered by the interpolation algorithms. Hence, the interpolation algorithms could be further improved, which might enhance their advantages over the SPPs.

5.2. Implications for hydrological modeling

The interpolated and the satellite-based spatially distributed precipitations were used to drive the fully distributed hydrological model DHSVM to assess their hydrological utilities. We found that DHSVM with the TMPA-based precipitation, even after the additional calibration, had overall a lower performance than that with the interpolated precipitation in modeling streamflow. This indicates that the interpolated precipitation, even from scarce rain gauges, should be more preferred than the TMPA-based one for streamflow simulations in the mountainous BRB. Regarding the IMERG-based precipitation, however, we found that the streamflow simulations accuracy could be higher than those with the interpolated precipitation during the validation

period, if DHSVM was subjected to additional calibration. This suggests that IMERG provides a valuable alternative for driving hydrological models to simulate streamflow over the data-scarce mountainous areas such as the BRB. In other words, IMERG could be used as a substitute to the gauge-based interpolated precipitation in case that only the streamflow is focused. The SPPs were proved to have a relatively low performance in capturing daily precipitation, but a good performance in estimating monthly precipitation. It could be inferred that they might be utilized to detect the trends of precipitation and streamflow, both of which are of great interest to the managers and policy makers. Fig. 8 depicts the variations and trends of the observed annual streamflows and the simulations generated in different experiments. We can see a consistent increasing trend for the period 2001–2007 together with a concurrent decreasing trend for the period 2007–2013, in line with the observations. This confirms the usefulness of the SPPs for determining the sign of streamflow trends, although not for accurately estimating the magnitudes of the trends. In other words, both the TMPA and IMERG products could be used as a substitute to the interpolated precipitation if the sign of streamflow trend is targeted. The above results also imply that the utilities of the SPPs depend heavily on the goals of the hydrological modeling.

It should be noticed that DHSVM with the TMPA-based or IMERG-based precipitation tends to exhibit different performance over different periods in simulating streamflow. Taking a closer look at the streamflow hydrography (Fig. 5), we can observe that the modeled streamflows in DHSVM-TMPA-UnCal are very close to DHSVM-PrecLaps and DHSVM-MicroMet for the years 2001, 2009 and 2012–2013 due to the similar precipitation estimates, but they were obviously overestimated in the years 2002–2007. The further model optimization in the experiment DHSVM-TMPA-Cal could therefore not consistently improve the streamflow simulation accuracy for all the years. Moreover, as listed in Table 4, the streamflow simulation accuracy in the experiment DHSVM-IMERG-UnCal/Cal is obviously better in the validation period than the calibration period. These results indicate that the hydrological utilities of the SPPs might vary for different time periods, underlining the necessity of conducting a hydrological evaluation of the SPPs for a relatively long period in order to give a more holistic assessment.

The hydrological utilities of the SPPs were typically assessed by using only the streamflow observations in many previous studies (e.g. Kim et al., 2016; Yan et al., 2017; Yuan et al., 2017; Li et al., 2018; Duan et al., 2019; Jiang and Bauer-Gottwein, 2019). In this study, we have also crosschecked the modeling results with the independent RS-based ET product. Interestingly, the simulated ET match well with the independent RS-based ET product ($NSE \geq 0.72$ and $R^2 \geq 0.85$) in the experiments DHSVM-PrecLaps, DHSVM-MicroMet, DHSVM-TMPA-UnCal and DHSV-IMERG-UnCal, although the streamflow simulation accuracy are obviously lower in the latter two experiments than the former two. The additional calibration of DHSVM with the TMPA-based or IMERG-based precipitation in the experiments DHSVM-TMPA-Cal or DHSVM-IMERG-Cal would enhance the streamflow simulation accuracy substantially, as presented in Section 4.2. However, the simulated summer ET would diverge more significantly from the RS-based ET estimates than those without additional calibration (i.e., DHSVM-TMPA-UnCal or DHSVM-IMERG-UnCal). Thus, the improvement of streamflow estimates is actually achieved by sacrificing the ET simulation accuracy, highlighting that the streamflow observations alone may not be adequate for evaluating the hydrological utilities of the SPPs. This also indicates that the hydrological model driven by the satellite-based precipitation, if calibrated solely against the streamflow observations, might not be adequate for water balance analyses or water accounting, since the precipitation estimation errors of the SPPs could be propagated to some other water balance components such as ET, as proven in this study.

5.3. Uncertainties

In this study, the observations of 12 rain gauges were used to assess the performance of two quasi-physically interpolation algorithms in and around the BRB through the leave-one-out cross-validation technique.

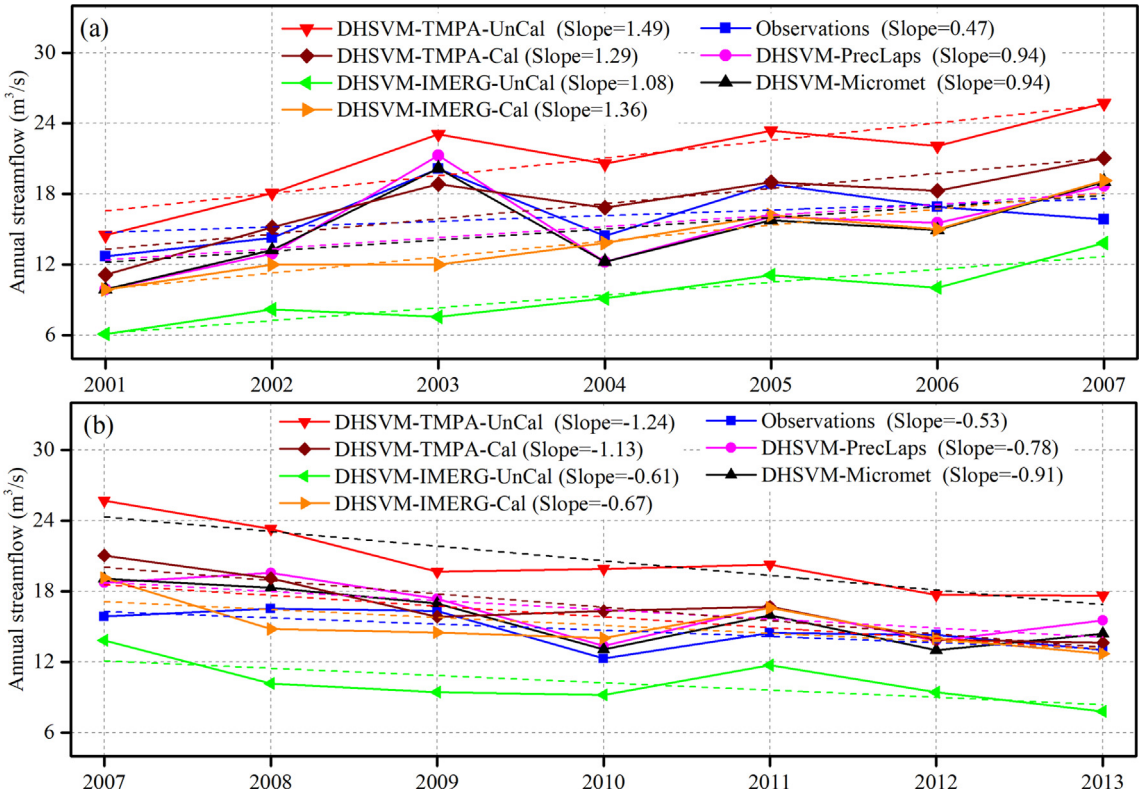

Fig. 8. Variations and trends of the observed and simulated annual streamflows for the two sub-periods 2001-2007 and 2007-2013.

The distances between two neighbor rain gauges are mostly less than 50 km, which could contribute to explain the reason why the interpolation algorithms could have better performances than the SPPs in capturing daily precipitation. However, the distribution of the rain gauges might be very sparse in some other regions such as the northwest Qinghai-Tibetan Platea. In this case, the interpolation algorithms may not still outperform the SPPs, particularly the IMERG product, considering that the nearest stations may not be able to represent the precipitation variations in the interpolated areas. There is another case that the rain gauges are very unevenly distributed in some large watersheds. In this case, the interpolation algorithm may not be able to capture the spatial variability of precipitation at the watershed scale, although it could have a higher performance than the SPPs when verified against the observations. Hence, the findings of the study might not be applicable to the regions with very sparse or unevenly distributed rain gauges, which necessitates further investigations in the future.

Rain gauge density was recognized as an important source of uncertainties in the evaluations of the SPPs (e.g. Amitai et al., 2012; Tang et al., 2018; Tian et al., 2018). In this study, we further assessed the performance of the interpolation algorithm (i.e., PrecLaps) and the SPPs (TMPA and IMERG) with the increasing numbers of rain gauges. More specifically, we used the five national-level meteorological stations as the baseline, and then randomly increased the number of rain gauges to the totally twelve. Because of the different combinations of the additional rain gauges, there would be some variations of the performance metrics. For instance, there would be totally 15 random combinations when two additional rain gauges are selected from the remaining six ones. The results are plotted in Fig. 9. We can see that, at the daily scale, the *CC* exhibits a consistent upward trend with the increasing number of rain gauges for the interpolation algorithm and the SPPs. Meanwhile, the *RMSE* shows an opposite downward trend. The results indicate that the performance of the interpolation algorithm and the SPPs would increase with more dense rain gauge network. Thus, if fewer rain gauges are utilized, the performance of the SPPs would be underestimated, as reported by Tang et al. (2018) and Tian et al. (2018). At the monthly scales, we can observe that there are no obvious trends of the *CC* and *RMSE* with the increasing number of rain gauges. This implies that the rain gauge density has a relatively low influence on the performance of the interpolation algorithms and the SPPs at the monthly scale. We can also see from Fig. 9 that the performance metrics of the interpolation algorithm show larger ranges for different combinations of the additional rain gauges, compared with those of the SPPs. This is due to the fact that the performance of the PrecLaps algorithm is not only intimately associated with the rain gauge density, but also with their distributions.

6. Conclusions

This study compared the performances of two quasi-physically based interpolation algorithms (i.e., MicroMet and PrecLaps) with the widely used SPPs (i.e., TMPA 3B42V7 and IMERG) at multiple time scales in and around the Babao River Basin (BRB), a meso-scale mountainous watershed on the northeast Qinghai Tibet Plateau. Meanwhile, the fully distributed hydrological model DHSVM was used to evaluate the hydrological utilities of the interpolated and the satellite-based precipitation through different modeling experiments (i.e., DHSVM-PrecLaps, DHSVM-MicroMet and DHSVM-TMPA-UnCal/Cal and DHSVM-IMERG-UnCal/Cal).

Results indicate that the SPPs perform worse than the interpolation algorithms in reproducing daily precipitation, while they show comparable and even higher performance in estimating monthly precipitation. At all the time scales, the IMERG product outperforms TMPA; and meanwhile, the MicroMet algorithm outperforms the

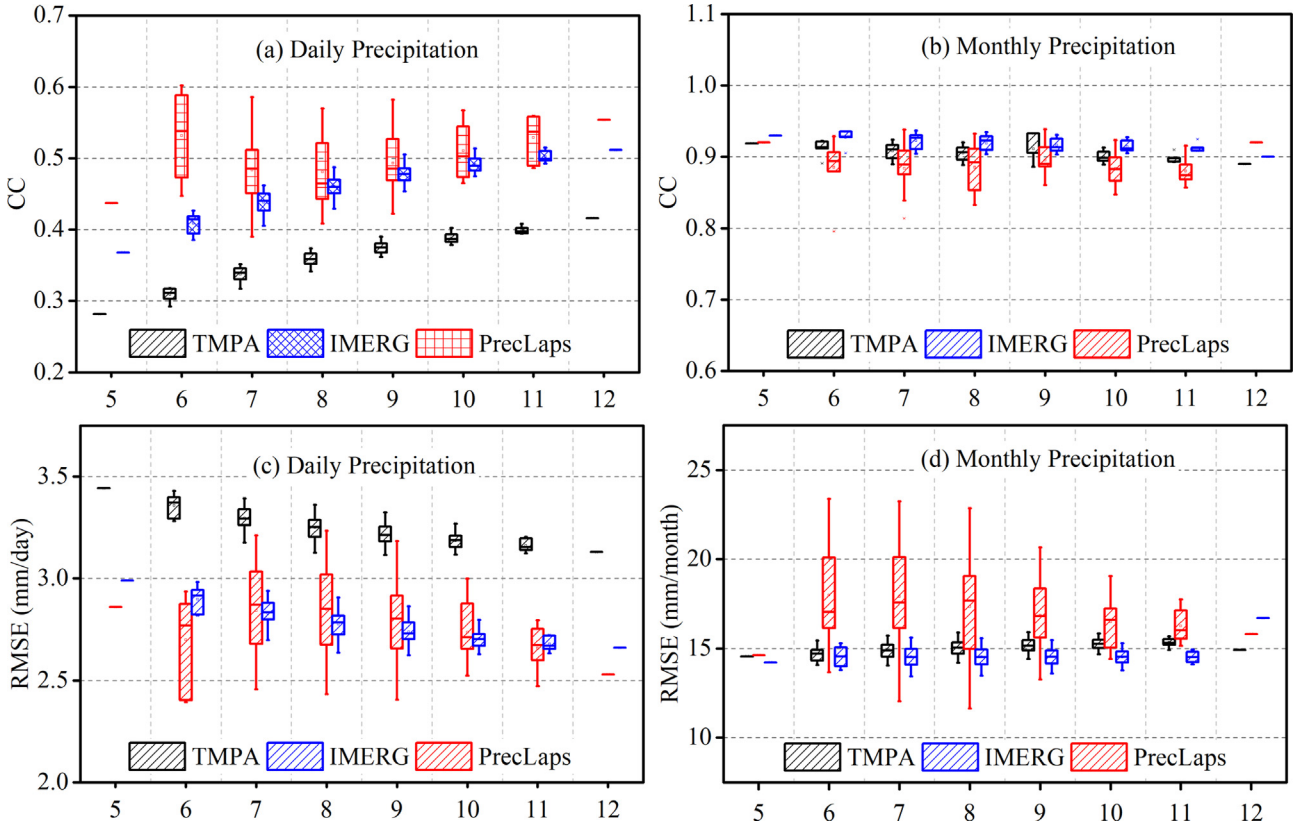

Fig. 9. Varying performance of the interpolation algorithm (PrecLaps) and the SPPs (TMPA and IMERG) with the increasing numbers of rain gauges. The box plots show the variations of the performance metrics resulting from different combinations of the additional rain gauges. The left and right columns present the results for the daily and monthly precipitation, respectively.

PrecLaps scheme. Both the interpolation algorithms and the SPPs exhibit an obvious seasonal variation regarding the performance, increasing from spring to summer and autumn, and then dropping rapidly in the cold winter. DHSVM with the TMPA-based or IMERG-based precipitation, when not subjected to additional calibration in the experiments DHSVM-TMPA-UnCal and DHSVM-IMERG-UnCal, has an apparent lower performance in simulating streamflow, compared to those with the interpolated precipitation in DHSVM-PrecLaps and DHSVM-MicroMet. However, interestingly, the ET simulations consistently agree well with the independent RS-based ET product in these experiments, as indicated by the higher performance metrics ($NSE \geq 0.72$ and $R^2 \geq 0.85$). The additional calibration of DHSVM with the TMPA-based or IMERG-based precipitation in DHSVM-TMPA-Cal and DHSVM-IMERG-Cal could enhance the streamflow simulation accuracy significantly. The *NSE* could increase by 70.59–109.52% and 86.84–132%, respectively, at the daily and monthly scales in the validation period. Nevertheless, the simulated summer ET would diverge more significantly from the RS-based ET product than those without additional calibration. The improvement of streamflow estimates is actually achieved by sacrificing the ET simulation accuracy, highlighting that the streamflow observations alone may not be adequate for evaluating the hydrological utilities of the SPPs, particularly if not only the streamflow but also some other water balance components are focused.

The further analyses revealed that the utilities of the SPPs depend heavily on the goals of the hydrological modeling. Moreover, the hydrological model with the satellite-based precipitation could have varying performance for different periods, implying the necessity of conducting a hydrological evaluation of the SPPs for a relatively long period. In addition, the performance of the SPPs and the interpolation algorithms are closely associated with the rain gauge density. One limitation of the study is that only one specific watershed was focused. Thus, further work needs to be carried out to verify whether our results can be generalized in some other mountainous watersheds with similar characteristics.

CRediT authorship contribution statement

Ling Zhang: Conceptualization, Formal analysis, Investigation, Funding acquisition, Methodology, Resources, Visualization, Writing - original draft, Writing - review & editing. **Dong Ren:** Investigation, Formal analysis, Resources, Writing - review & editing. **Zhuotong Nan:** Resources, Supervision, Writing - review & editing. **Weizhen Wang:** Resources, Supervision, Writing - review & editing. **Yi Zhao:** Investigation, Software, Resources. **Yanbo Zhao:** Investigation, Validation, Writing - review & editing. **Qimin Ma:** Investigation, Validation, Writing - review & editing. **Xiaobo Wu:** Investigation, Validation, Writing - review & editing.

Declaration of Competing Interest

The authors declare that they have no known competing financial interests or personal relationships that could have appeared to influence the work reported in this paper.

Acknowledgements

This study was supported by the Strategic Priority Research Program of Chinese Academy of Sciences (XDA19040504 and XDA20100104), the National Natural Science Foundation of China (41901045 and 41471448), and the CAS “Light of West China” Program (29Y929661). The authors would like to thank the UW Hydro Computational Hydrology group at the University of Washington for providing the source codes of DHSVM. The authors also wish to express their gratitude to the anonymous reviewers for their valuable comments and suggestions on the paper.

References

Alvarenga, L.A., de Mello, C.R., Colombo, A., et al., 2018. Impacts of climate change on the hydrology of a Small Brazilian headwater catchment using the distributed hydrology-soil-vegetation model. Am. J. Clim. Change 07 (02), 355–366. https://doi.org/10.4236/ajcc.2018.72021.

Amitai, E., Unkrich, C.L., Goodrich, D.C., et al., 2012. Assessing satellite-based rainfall estimates in semiarid watersheds using the USDA-ARS walnut gulch gauge network and TRMM PR. J. Hydrometeorol. 13 (5), 1579–1588. https://doi.org/10.1175/JHM-D-12-016.1.

Bárdossy, A., Pegram, G., 2013. Interpolation of precipitation under topographic influence at different time scales. Water Resour. Res. 49 (8), 4545–4565. https://doi.org/10.1002/wrcr.20307.

Beck, H.E., Pan, M., Roy, T., et al., 2019. Daily evaluation of 26 precipitation datasets using Stage-IV gauge-radar data for the CONUS. Hydrol. Earth Syst. Sc. 23 (1), 207–224. https://doi.org/10.5194/hess-23-207-2019.

Belabid, N., Zhao, F., Brocca, L., et al., 2019. Near-real-time flood forecasting based on satellite precipitation products. Remote Sens. 11 (3), 252. https://doi.org/10.3390/rs11030252.

Bharti, V., Singh, C., 2015. Evaluation of error in TRMM 3B42V7 precipitation estimates over the Himalayan region. J. Geophys. Res. Atmos. 120 (24), 12458–12473. https://doi.org/10.1002/2015JD023779.

Camera, C., Bruggeman, A., Hadjinicolaou, P., et al., 2014. Evaluation of interpolation techniques for the creation of gridded daily precipitation (1 × 1 km2); Cyprus, 1980–2010. J. Geophys. Res. Atmos. 119 (2), 693–712.

Camici, S., Ciabatta, L., Massari, C., et al., 2018. How reliable are satellite precipitation estimates for driving hydrological models: a verification study over the Mediterranean area. J. Hydrol. 563, 950–961. https://doi.org/10.1016/j.jhydrol.2018.06.067.

Cao, Y., Nan, Z., Cheng, G., et al., 2018. Hydrological variability in the Arid Region of Northwest China from 2002 to 2013. Adv. Meterol. 2018, 1–13. https://doi.org/10.1155/2018/1502472.

Cuo, L., Lettenmaier, D.P., Mattheussen, B.V., et al., 2008. Hydrologic prediction for urban watersheds with the Distributed Hydrology-Soil-Vegetation Model. Hydrol. Processes 22 (21), 4205–4213.

Delrieu, G., Berne, A., Borga, M., et al., 2009. Weather radar and hydrology. Adv. Water Res. 7 (32), 969–974. https://doi.org/10.1016/j.advwatres.2009.03.006.

Du, J., Xie, S., Xu, Y., et al., 2007. Development and testing of a simple physically-based distributed rainfall-runoff model for storm runoff simulation in humid forested basins. J. Hydrol. 336 (3–4), 334–346. https://doi.org/10.1016/j.jhydrol.2007.01.015.

Duan, Z., Tuo, Y., Liu, J., et al., 2019. Hydrological evaluation of open-access precipitation and air temperature datasets using SWAT in a poorly gauged basin in Ethiopia. J. Hydrol. 569, 612–626. https://doi.org/10.1016/j.jhydrol.2018.12.026.

Ebrahimi, S., Chen, C., Chen, Q., et al., 2017. Effects of temporal scales and space mismatches on the TRMM 3B42 v7 precipitation product in a remote mountainous area. Hydrol. Processes 31 (24), 4315–4327. https://doi.org/10.1002/hyp.11357.

El Kenawy, A.M., Lopez-Moreno, J.I., McCabe, M.F., et al., 2015. Evaluation of the TMPA-3B42 precipitation product using a high-density rain gauge network over complex terrain in northeastern Iberia. Global Planet. Change 133, 188–200. https://doi.org/10.1016/j.gloplacha.2015.08.013.

Garen, D.C., Johnson, G.L., Hanson, C.L., 1994. Mean areal precipitation for daily hydrologic modeling in mountainous regions1. J. Am. Water Resour. As. 30 (3), 481–491. https://doi.org/10.1111/j.1752-1688.1994.tb03307.x.

Gritti, E.S., Smith, B., Sykes, M.T., 2006. Vulnerability of Mediterranean Basin ecosystems to climate change and invasion by exotic plant species. J. Bliogeor. 33 (1), 145–157. https://doi.org/10.1111/j.1365-2699.2005.01377.x.

Huang, H., Liang, Z., Li, B., et al., 2019. A new spatial precipitation interpolation method based on the information diffusion principle. Stoch. Env. Res. Risk A 33 (3), 765–777. https://doi.org/10.1007/s00477-019-01658-2.

Huffman, G.J., Bolvin, D.T., Nelkin, E.J., et al., 2007. The TRMM Multisatellite Precipitation Analysis (TMPA): quasi-global, multiyear, combined-sensor precipitation estimates at fine scales. J. Hydrometeorol. 8 (1), 38–55. https://doi.org/10.1175/JHM560.1.

Huffman, G., Bolvin, D., Braithwaite, D. et al., 2014. Integrated Multi-satellitE Retrievals for GPM (IMERG), version 4.4. NASA's Precipitation Processing Center, accessed 31 March, 2015, ftp://arthurhou.pps.eosdis.nasa.gov/gpmdata/.

Hui-Mean, F., Yusop, Z., Yusof, F., 2018. Drought analysis and water resource availability using standardised precipitation evapotranspiration index. Atmos. Res. 201, 102–115. https://doi.org/10.1016/j.atmosres.2017.10.014.

Hussain, S., Song, X., Ren, G., et al., 2017. Evaluation of gridded precipitation data in the Hindu Kush–Karakoram–Himalaya mountainous area. Hydrol. Sci. J. 62 (14), 2393–2405. https://doi.org/10.1080/02626667.2017.1384548.

Hwang, Y., Clark, M., Rajagopalan, B., et al., 2012. Spatial interpolation schemes of daily precipitation for hydrologic modeling. Stoch. Env. Res. Risk A 26 (2), 295–320. https://doi.org/10.1007/s00477-011-0509-1.

Jia, L., Shang, H., Hu, G., et al., 2011. Phenological response of vegetation to upstream river flow in the Heihe Rive basin by time series analysis of MODIS data. Hydrol. Earth Syst. Sc. 15 (3), 1047–1064. https://doi.org/10.5194/hess-15-1047-2011.

Jiang, L., Bauer-Gottwein, P., 2019. How do GPM IMERG precipitation estimates perform as hydrological model forcing? Evaluation for 300 catchments across Mainland China. J. Hydrol. 572, 486–500. https://doi.org/10.1016/j.jhydrol.2019.03.042.

Khan, A., Koch, M., Chinchilla, K., 2018. Evaluation of Gridded Multi-Satellite Precipitation Estimation (TRMM-3B42-V7) Performance in the Upper Indus Basin (UIB). Climate 6 (3), 76. https://doi.org/10.3390/cli6030076.

Kim, J., Jung, I., Park, K., et al., 2016. Hydrological utility and uncertainty of multi-

satellite precipitation products in the mountainous region of South Korea. Remote Sens. 8 (7), 608. https://doi.org/10.3390/rs8070608.
Koch, S.E., desJardins, M., Kocin, P.J., 1983. An interactive Barnes objective map analysis scheme for use with satellite and conventional data. J. Climate Appl. Meteor. 22 (9), 1487–1503. https://doi.org/10.1175/1520-0450(1983) 022<1487:AIBOMA>2.0.CO;2.
Kummerow, C., Barnes, W., Kozu, T., et al., 1998. The Tropical Rainfall Measuring Mission (TRMM) Sensor Package. J. Atmos. Oceanic Technol. 15 (3), 809–817. https://doi.org/10.1175/1520-0426(1998) 015<0809:TTRMMT>2.0.CO;2.
Lanini, J.S., Clark, E.A., Lettenmaier, D.P., 2009. Effects of fire-precipitation timing and regime on post-fire sediment delivery in Pacific Northwest forests. Geophys. Res. Lett. 36. https://doi.org/10.1029/2008GL034588.
Li, D., Christakos, G., Ding, X., et al., 2018. Adequacy of TRMM satellite rainfall data in driving the SWAT modeling of Tiaoxi catchment (Taihu lake basin, China). J. Hydrol. 556, 1139–1152. https://doi.org/10.1016/j.jhydrol.2017.01.006.
Li, Z., Yang, D., Gao, B., et al., 2015. Multiscale hydrologic applications of the latest satellite precipitation products in the Yangtze River Basin using a Distributed Hydrologic Model. J. Hydrometeorol. 16 (1), 407–426. https://doi.org/10.1175/JHM-D-14-0105.1.
Liang, X., Lettenmaier, D.P., Wood, E.F., et al., 1994. A simple hydrologically based model of land surface water and energy fluxes for general circulation models. J. Geophys. Res. Atmos. 99 (D7), 14415–14428.
Lima, G.N.d., Lombardo, M.A., Magaña, V., 2018. Urban water supply and the changes in the precipitation patterns in the metropolitan area of São Paulo-Brazil. Appl. Geogr. 94, 223–229. https://doi.org/10.1016/j.apgeog.2018.03.010.
Liston, G.E., Elder, K., 2006. A meteorological distribution system for high-resolution terrestrial modeling (MicroMet). J. Hydrometeorol. 7 (2), 217–234.
Lu, L., Liu, C., Li, X., 2011. Soil texture dataset of the Heihe river basin (2011). Heihe Plan Sci. Data Center. https://doi.org/10.3972/heihe.023.2013.db.
Meng, J., Li, L., Hao, Z., et al., 2014. Suitability of TRMM satellite rainfall in driving a distributed hydrological model in the source region of Yellow River. J. Hydrol. 509, 320–332. https://doi.org/10.1016/j.jhydrol.2013.11.049.
Mernild, S.H., Liston, G.E., Hiemstra, C., et al., 2017. The Andes Cordillera. Part III: glacier surface mass balance and contribution to sea level rise (1979–2014). Int. J. Climatol. 37 (7), 3154–3174. https://doi.org/10.1002/joc.4907.
Mo, K., Chen, Q., Chen, C., et al., 2019. Spatiotemporal variation of correlation between vegetation cover and precipitation in an arid mountain-oasis river basin in northwest China. J. Hydrol. 574, 138–147. https://doi.org/10.1016/j.jhydrol.2019.04.044.
Nash, J.E., Sutcliffe, J.V., 1970. River flow forecasting through conceptual models part I — a discussion of principles. J. Hydrol. 10 (3), 282–290. https://doi.org/10.1016/0022-1694(70)90255-6.
Ossa-Moreno, J., Keir, G., McIntyre, N., et al., 2019. Comparison of approaches to interpolating climate observations in steep terrain with low-density gauging networks. Hydrol. Earth Syst. Sci. 23 (11), 4763–4781. https://doi.org/10.5194/hess-23-4763-2019.
Peng, B., Shi, J., Ni-Meister, W., et al., 2014. Evaluation of TRMM Multisatellite Precipitation Analysis (TMPA) Products and Their Potential Hydrological Application at an Arid and Semiarid Basin in China. IEEE J. Selected Top. Appl. Earth Observ. Remote Sens. 7 (9), 3915–3930. https://doi.org/10.1109/JSTARS.2014.2320756.
Saltelli, A., Tarantola, S., Chan, K.P.S., 1999. A quantitative model-independent method for global sensitivity analysis of model output. Technometrics 41 (1), 39. https://doi.org/10.1080/00401706.1999.10485594.
Sheng, Y., Pan, Y., Yu, J., et al., 2013. Quality assessment of hourly merged precipitation product over China (in Chinese). Trans. Atmos. Sci. 36 (1), 37–46.
Song, X.-D., Brus, D.J., Liu, F., et al., 2016. Mapping soil organic carbon content by geographically weighted regression: a case study in the Heihe River Basin, China. Geoderma 261, 11–22. https://doi.org/10.1016/j.geoderma.2015.06.024.
Storck, P., Bowling, L., Wetherbee, P., et al., 1998. Application of a GIS-based distributed hydrology model for prediction of forest harvest effects on peak stream flow in the Pacific Northwest. Hydrol. Processes 12 (6), 889–904.
Sun, Q., Miao, C., Duan, Q., et al., 2018. A review of global precipitation data sets: data sources, estimation, and intercomparisons. Rev. Geophys. 56 (1), 79–107. https://doi.org/10.1002/2017RG000574.
Supit, I., van Diepen, C.A., de Wit, A.J.W., et al., 2012. Assessing climate change effects on European crop yields using the Crop Growth Monitoring System and a weather generator. Agric. For. Meteorol. 164, 96–111. https://doi.org/10.1016/j.agrformet.2012.05.005.
Tang, G., Ma, Y., Long, D., et al., 2016. Evaluation of GPM Day-1 IMERG and TMPA Version-7 legacy products over Mainland China at multiple spatiotemporal scales. J. Hydrol. 533, 152–167. https://doi.org/10.1016/j.jhydrol.2015.12.008.
Tang, G., Behrangi, A., Long, D., et al., 2018. Accounting for spatiotemporal errors of gauges: a critical step to evaluate gridded precipitation products. J. Hydrol. 559, 294–306. https://doi.org/10.1016/j.jhydrol.2018.02.057.
Thornton, P.E., Running, S.W., White, M.A., 1997. Generating surfaces of daily meteorological variables over large regions of complex terrain. J. Hydrol. 190 (3), 214. https://doi.org/10.1016/S0022-1694(96)03128-9.
Tian, F., Hou, S., Yang, L., et al., 2018. How does the evaluation of the GPM IMERG rainfall product depend on gauge density and rainfall intensity? J. Hydrometeorol. 19 (2), 339–349. https://doi.org/10.1175/JHM-D-17-0161.1.
Tobin, C., Nicotina, L., Parlange, M.B., et al., 2011. Improved interpolation of meteorological forcings for hydrologic applications in a Swiss Alpine region. J. Hydrol. 401 (1–2), 77–89. https://doi.org/10.1016/j.jhydrol.2011.02.010.
Wang, X., Ding, Y., Zhao, C., et al., 2019. Similarities and improvements of GPM IMERG upon TRMM 3B42 precipitation product under complex topographic and climatic conditions over Hexi region, Northeastern Tibetan Plateau. Atmos. Res. 218, 347–363. https://doi.org/10.1016/j.atmosres.2018.12.011.
Wang, C., Tang, G., Han, Z., et al., 2018. Global intercomparison and regional evaluation of GPM IMERG Version-03, Version-04 and its latest Version-05 precipitation products: similarity, difference and improvements. J. Hydrol. 564, 342–356. https://doi.org/10.1016/j.jhydrol.2018.06.064.
Wang, Y., Yang, D., Lei, H., et al., 2015. Impact of cryosphere hydrological processes on the river runoff in the upper reaches of Heihe River (in Chinese). J. Hydraul. Eng. 46 (9), 1064–1071.
Wigmosta, M.S., Perkins, W.A., 2001. Simulating the effects of forest roads on watershed hydrology. Land Use Watersheds: Hum. Influence Hydrol. Geomorphol. Urban Forest Areas 127–143. https://doi.org/10.1029/WS002p0127.
Wigmosta, M.S., Vail, L.W., Lettenmaier, D.P., 1994. A distributed hydrology-vegetation model for complex terrain. Water Resour. Res. 30 (6), 1665–1679.
Wu, B., Yan, N., Xiong, J., et al., 2012. Validation of ETWatch using field measurements at diverse landscapes: a case study in Hai Basin of China. J. Hydrol. 436–437, 67–80. https://doi.org/10.1016/j.jhydrol.2012.02.043.
Xu, R., Tian, F., Yang, L., et al., 2017. Ground validation of GPM IMERG and TRMM 3B42V7 rainfall products over southern Tibetan Plateau based on a high-density rain gauge network. J. Geophys. Res. Atmos. 122 (2), 910–924. https://doi.org/10.1002/2016JD025418.
Xu, W., Zou, Y., Zhang, G., et al., 2015. A comparison among spatial interpolation techniques for daily rainfall data in Sichuan Province, China. Int. J. Climatol. 35 (10), 2898–2907. https://doi.org/10.1002/joc.4180.
Yan, D., Liu, S., Qin, T., et al., 2017. Evaluation of TRMM precipitation and its application to distributed hydrological model in Naqu River Basin of the Tibetan Plateau. Hydrol. Res. 48 (3), 822–839. https://doi.org/10.2166/nh.2016.090.
Yang, Y., Tang, J., Xiong, Z., et al., 2017. Evaluation of high-resolution gridded precipitation data in arid and semiarid regions: Heihe River Basin, Northwest China. J. Hydrometeorol. 18 (12), 3075–3101. https://doi.org/10.1175/JHM-D-16-0252.1.
Yang, R.-M., Zhang, G.-L., Liu, F., et al., 2016. Comparison of boosted regression tree and random forest models for mapping topsoil organic carbon concentration in an alpine ecosystem. Ecol. Indic. 60, 870–878. https://doi.org/10.1016/j.ecolind.2015.08.036.
Yearsley, J.R., Sun, N., Baptiste, M., et al., 2019. Assessing the impacts of hydrologic and land use alterations on water temperature in the Farmington River Basin in Connecticut. Hydrol. Earth Syst. Sci. Discuss. 1–34. https://doi.org/10.5194/hess-2019-94.
Yong, B., Liu, D., Gourley, J.J., et al., 2015. Global view of real-time trmm multisatellite precipitation analysis: implications for its successor global precipitation measurement mission. Bull. Am. Meteorol. Soc. 96 (2), 283–296. https://doi.org/10.1175/BAMS-D-14-00017.1.
Yuan, F., Zhang, L., Win, K., et al., 2017. Assessment of GPM and TRMM multi-satellite precipitation products in streamflow simulations in a data-sparse mountainous watershed in Myanmar. Remote Sens. 9 (3), 302. https://doi.org/10.3390/rs9030302.
Yuan, F., Wang, B., Shi, C., et al., 2018. Evaluation of hydrological utility of IMERG Final run V05 and TMPA 3B42V7 satellite precipitation products in the Yellow River source region, China. J. Hydrol. 567, 696–711. https://doi.org/10.1016/j.jhydrol.2018.06.045.
Yuan, F., Zhang, L., Soe, K., et al., 2019. Applications of TRMM- and GPM-Era multiple-satellite precipitation products for flood simulations at sub-daily scales in a sparsely gauged watershed in Myanmar. Remote Sens. 11 (2), 140. https://doi.org/10.3390/rs11020140.
Zhang, Y., Cheng, G., Li, X., et al., 2017b. Influences of frozen ground and climate change on hydrological processes in an alpine watershed: a case study in the upstream area of the Hei'he River, Northwest China. Permafrost Reriglac. 28 (2), 420–432. https://doi.org/10.1002/ppp.1928.
Zhang, L., He, C., Li, J., et al., 2017a. Comparison of IDW and physically based IDEW method in hydrological modelling for a large mountainous watershed, Northwest China. River Res. Appl. 33 (6), 912–924. https://doi.org/10.1002/rra.3147.
Zhang, G., Kang, S., Cuo, L., et al., 2016. Modeling hydrological process in a glacier basin on the central Tibetan Plateau with a distributed hydrology soil vegetation model. J. Geophys. Res. Atmos. 121 (16), 9521–9539. https://doi.org/10.1002/2016JD025434.
Zhang, L., Nan, Z., Yu, W., et al., 2018b. Comparison of baseline period choices for separating climate and land use/land cover change impacts on watershed hydrology using distributed hydrological models. Sci. Total Environ. 622–623, 1016–1028. https://doi.org/10.1016/j.scitotenv.2017.12.055.
Zhang, L., Nan, Z., Liang, X., et al., 2018a. Application of the MacCormack scheme to overland flow routing for high-spatial resolution distributed hydrological model. J. Hydrol. 558, 421–431. https://doi.org/10.1016/j.jhydrol.2018.01.048.
Zhang, X., Zhou, J., Cai, W., et al., 2018c. Vegetation mapping (1:100000) in Heihe River Basin using 3S technology (in Chinese). J. Northwest Normal Univ. (Natural Sci.) 54 (2), 95–101.
Zhao, Y., Nan, Z., Yu, W., et al., 2019. Calibrating a hydrological model by stratifying frozen ground types and seasons in a cold alpine Basin. Water. https://doi.org/10.3390/w11050985.
Zheng, D., van der Velde, R., Su, Z., et al., 2018. Impact of soil freeze-thaw mechanism on the runoff dynamics of two Tibetan rivers. J. Hydrol. 563, 382–394. https://doi.org/10.1016/j.jhydrol.2018.06.024.